Reply to Referee#1:

General Comments:

In this study, an aging and optical change of organic tar particles in the regional haze was observed. Domestic coal and biomass burning are suggested to be the important reasons for haze formation in the NCP. It is found that with the evolution of haze, organic particles decreased, secondary inorganic aerosol increased, POT-SIA particles increased, and POT (primary organic tar) particles decreased, indicating that POT particles could provide surface for heterogeneous reactions of SO_2 and NO_x. It is also concluded that POT particles are coated with secondary inorganic aerosol, which leads to increased light absorption of particulate. Therefore, the "lensing effect" should be further considered on the POT particles in radiative forcing models. The results obtained in this study are interesting and worthy to be published in ACP.

Response: We appreciated referee#1's careful reading and positive feedback. All the comments and suggestions are valuable for improving the quality of our paper. Our point-to-point replies to the referee's comments are listed below and the changes are incorporated into the revised manuscript marked in red color.

Specific Comments:

1. The diagrams are too complex to understand, and some of the parameters in the diagrams have not been analyzed. For example, the mass concentrations of CO and NO_2 in Figure 2.

   Response: According to the referee's suggestion, we redraw the figures. Because the variations of the gaseous pollutants were used in this manuscript only to help understand the evolution of haze episodes, they were not the main concerns of this manuscript, therefore we did not discuss them in detail and we moved the lines of gaseous pollutants in Figure 2 into the Supplementary Information (Figure S2) to make the figure more concise to read.

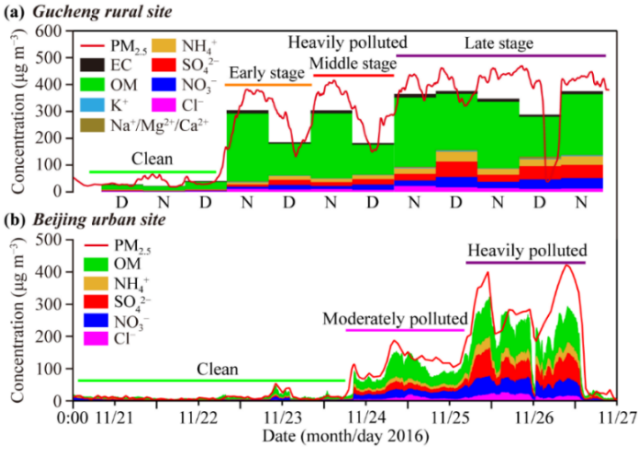

Figure 2

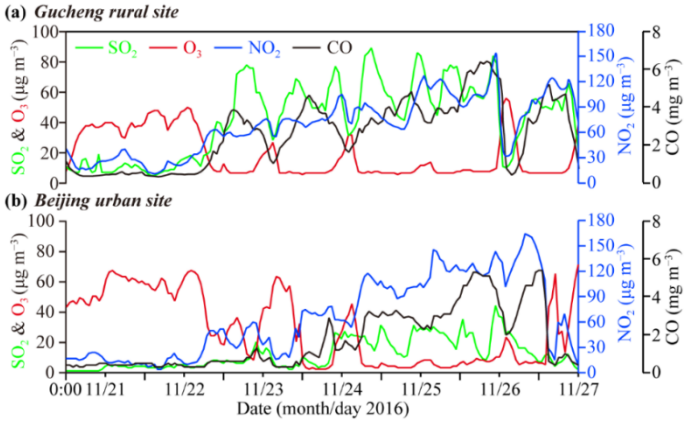

Figure S2

2. The offline bulk sample analysis is used for rural site while the online analysis is used for urban site. Can the values from two methods for the two sites be compared? Are there any errors or deviations between the results from offline bulk sample analysis and online analysis for urban site?

Response: Thanks for the comment. In this paper, we mainly focused on the microscopic properties and aging process of primary organic particles through the individual particle analysis. Due to the limited instruments, we collected offline $PM_{2.5}$ filter samples at the Gucheng rural site and used the Aerosol Mass Spectrometer (AMS) to continuously monitor the chemical species at the Beijing urban site. The bulk analysis results were used as solid evidence to support the individual particle analysis results. We mainly focused on the relative changes of different chemical species but not the absolute concentration changes. The detailed comparison of bulk analysis results between the two sites is not intended. Therefore, we did not compare the bulk analysis results between the two sites in this paper. The deviations between the offline bulk sample analysis and the online analysis at the urban site were not determined because of the lack of offline samples.

3. The analysis shows that fossil fuel burning and biomass burning are the main sources of pollution. What is the difference between POT particles produced by these two sources?

   Response: The previous papers reported that tar balls can be emitted from biomass burning (Pósfai et al., *J. Geophys. Res.*, 108, D13, 8483, 2003) and coal combustion (Zhang et al., *J. Geophys. Res.*, 123, 12964-12979, 2018). These papers reported similar characteristics such as spherical morphology, high viscosity, and C/O composition of tar balls. Therefore, it is difficult to distinguish the tar balls emitted from biomass burning and coal combustion, which is out of the main objective of this manuscript. Therefore, we did not identify their exact sources, and as referee#2 suggested, we refer to them as the burning-related primary organic particles. We think that the reviewer's comments might be our next aim to work on it.

   References:

   Pósfai, M., Simonics, R., Li, J., Hobbs, P. V., and Buseck, P. R.: Individual aerosol particles from biomass burning in southern Africa: 1. Compositions and size distributions of carbonaceous particles, J. Geophys. Res.-Atmos., 108, 8483, 10.1029/2002JD002291, 2003.

   Zhang, Y., Yuan, Q., Huang, D., Kong, S., Zhang, J., Wang, X., Lu, C., Shi, Z., Zhang, X., Sun, Y., Wang, Z., Shao, L., Zhu, J., and Li, W.: Direct observations of fine primary particles from residential coal burning: insights into their morphology, composition, and hygroscopicity, J. Geophys. Res.-Atmos., 123, 12964-12979, 10.1029/2018JD028988, 2018.

4. It is concluded that the particle size of the rural point is larger than that of the urban point, because the particles with small particle size are easier to be transmitted. However, in this transportation process, the formation of new particles or secondary chemical reaction (aging) may occur, which would increase the particle sizes, do the authors take into account this factor.

   Response: We appreciate the referee's comment. Indeed, the whole aged particle sizes increased due to the production of secondary aerosols on their surfaces during the particle aging process as we have shown in the manuscript. What we refer to is that the sizes of uncoated POA particles slightly decreased during the regional transport.

5. The second paragraph of the conclusion: "The primary pollutants from the intense coal and biomass burning in rural areas can also pose serious threats to human

health……". This looks unnecessary as the health effects are not the focus of this current study and it may need to be removed.

Response: According to the referee's suggestion, we removed this part.

6. Line 251 "Figure S2a shows higher fractions of OM, EC, and Cl^- at nighttime than daytime during the whole haze episode at the GC rural site, suggesting the continuous strong local combustion emissions at nighttime". We notice that the whole haze period was from November 22 to 27, and Figure 2A shows that the EC quality score was higher at nighttime than in the daytime on November 22. Please also explain why the nighttime would have higher level combustion emissions.

   Response: As we have written in the manuscript, at the GC rural site the $PM_{2.5}$ concentration began to increase at 18:00 on 22 November and the air quality was changed from the clean period to heavily polluted period during the 22–27 November. The EC concentration at the nighttime (12.1 μg m^{-3}) was much higher than that (1.8 μg m^{-3}) in the daytime on November 22 (Figure 2a). In rural areas, people may work out and the heating activities stopped in the daytime. But at nighttime people all stayed at home and consumed more biomass and coal for cooking and heating, especially the heating activities with coal maintained several hours during the nighttime, which can release large amounts of pollutants into the air. Therefore, the primary emissions were much higher during the daytime than the nighttime.

7. Figure S2b shows only the ion concentration of 5 parameters, and the concentration of other ions at the rural points should also be listed.

   Response: As we have mentioned above, at the Gucheng rural site, offline $PM_{2.5}$ filter samples were collected to obtain the concentrations of water-soluble inorganic ions (i.e., Cl^-, SO_4^{2-}, NO_3^-, Na^+, NH_4^+, K^+, Mg^{2+}, and Ca^{2+}) using the ion chromatograph and obtain the OC and EC concentrations using the OC/EC analyzer. However, at the Beijing urban site offline $PM_{2.5}$ filter samples were not collected. Instead, we used the online Aerosol Mass Spectrometer (AMS) which can only obtain five chemical species (i.e., OM, Cl^-, SO_4^{2-}, NO_3^-, and NH_4^+). Therefore, we provided 10 chemical species at the Gucheng rural site and five chemical species at the Beijing urban site. We should note that the lack of Na^+, Mg^{2+}, Ca^{2+}, K^+, and EC at the Beijing urban site did not influence the main content and conclusions of this paper, because the primary organic aerosols and secondary

inorganic aerosols were mainly discussed in this study.

8. It is better to have discrimination of the ion concentration between daytime and nighttime for Figure S2 and Figure 2. In addition, the variation trend of CO concentration in Figure 2 may needs to be put together with gaseous pollutants such as SO_2 and O_3.

   Response: According to the referee's suggestion, we added the comparison of chemical species concentrations between the daytime and nighttime, also we put the CO line with gaseous pollutants together. Moreover, the figure showing variation trends of gaseous pollutants were moved to the Supplementary Information (Figure S2), as has mentioned in question 1.

9. The specific calculation formula of light absorption cross section needs to be provided in methodology section.

   Response: As the reviewer suggested, we provided the calculation formula of light absorption cross sections in the methodology section.

   Please refer to Line 211-222 :

   After running the Mie calculation, the attenuation efficiency (Q_{atn}), scattering efficiency (Q_{sca}), and absorption efficiency (Q_{abs}) of an individual particle were output with their definitions as follows (Aden and Kerker, 1951; Toon and Ackerman, 1981):

$$Q_{atn} = \left(\frac{2}{x^2}\right) \sum_{n=1}^{\infty} (2n+1)[\mathrm{Re}(a_n + b_n)] \qquad (1)$$

$$Q_{sca} = \left(\frac{2}{x^2}\right) \sum_{n=1}^{\infty} (2n+1)(|a_n|^2+|b_n|^2) \qquad (2)$$

$$Q_{abs} = Q_{atn} - Q_{sca} \qquad (3)$$

   where $x = \frac{\pi D}{\lambda}$, is the dimensionless size parameter of the particle diameter D and the wavelength of light λ; a_n and b_n are calculated from Riccati–Bessel functions of the particles sizes and refractive indices (Bohren and Huffman, 1983); The symbol Re denotes the real part of the complex quantity a_n+b_n.

   The ACS of a particle can be obtained via multiplying the Q_{abs} by the geometric cross section of the particle as follow:

$$\mathrm{ACS} = Q_{abs} \times \frac{\pi D^2}{4} \qquad (4)$$

   References:

Aden, A. L., and Kerker, M.: Scattering of Electromagnetic Waves from Two Concentric Spheres, Journal of Applied Physics, 22, 1242-1246, 10.1063/1.1699834, 1951.

Toon, O. B., and Ackerman, T. P.: Algorithms for the calculation of scattering by stratified spheres, Appl. Opt., 20, 3657-3660, 10.1364/ao.20.003657, 1981.

Bohren, C. F., and Huffman, D. R.: Absorption and scattering of light by small particles, John Wiley & Sons, New York, 1983.

10. Figure 9. Legend error. Ratio should be replaced by Eabs.

Response: Corrected.

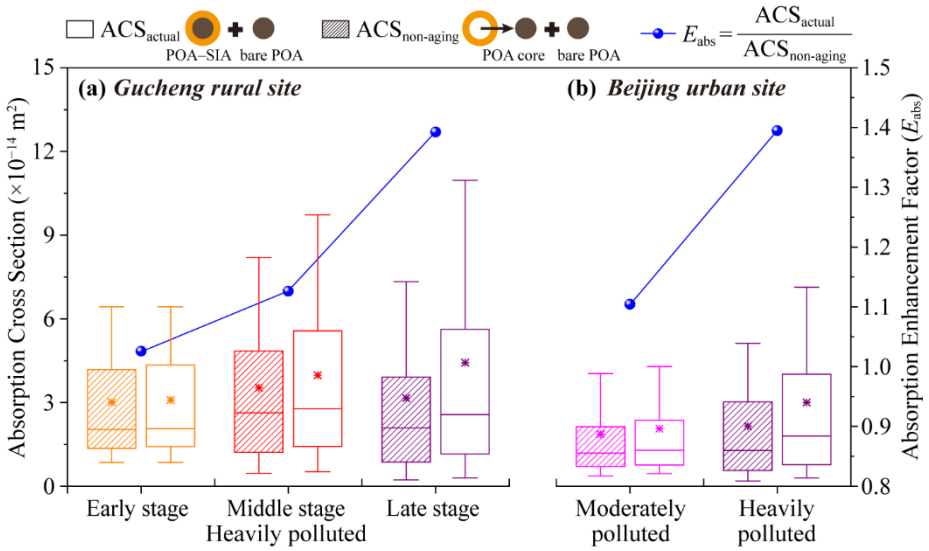

11. Line 390: “pore” may be core.

Response: Corrected.

Reply to Referee#2:

General Comments:

This study describes and compares wintertime aerosol particles in a rural location on the North China Plain with aerosol in Beijing (downwind from the rural site): aerosol concentration, chemical composition and individual-particle properties were measured, and optical properties simulated. The measurement campaign covered a period when conditions changed from relatively clean to heavily polluted, and the aerosol at the assumed source (the rural site) and in the urban haze could be compared. The major finding is that refractory primary organic particles from coal and biomass burning dominate at the rural site, and similar but coated particles are the major constituents in the aged haze. The inorganic coatings change the optical properties of the aerosol, by enhancing their absorption. The paper is sound and fairly well written. I have three concerns, one of which is partly a terminological issue.

Response: We thank referee#2' careful reading and critical comments which are helpful for improving the quality of our paper. All the comments and concerns raised by the referee have been explicitly considered and incorporated into the revised manuscript marked in red color.

Specific Comments:

1. Primary Organic Tar (POT). I am slightly uncomfortable with the use of the term "primary organic tar" (and its acronym, POT) for the observed class of particles. From the results it seems a correct interpretation that these particles are primary organics emitted by burning of coal and biomass. However, this is an interpretation and not an observation, as is now presented right at the start of the paper. The properties we know from TEM include the morphologies of the particles (some spherical and others irregular), their C-rich nature (although the particles were collected on a thick carbon+plastic film and therefore we do not know how much C they contain), and their thickness from SEM which suggests they were quite viscous when they arrived onto the grids. Indeed, these properties and the high concentrations at the locality where burning of coal is a major source of particles suggests they are primary organics. However, I am not sure they can be called "tar", since there is no study of the speciation of their components (although the authors refer to Xu et al. 2019 who used AMS and identified three groups of burning-related

factors). Admittedly, "tar" is a vaguely defined substance. However, the atmospheric chemistry literature is already replete with vaguely defined terms (and acronyms), and introducing a new one, such as POT may not help to clear the confusion. For the spherical types of such particles already exists a widely used term, "tar ball". And about tar balls we know they are primary (Tóth et al. ACP 14, 6669–6675, 2014), indeed made of tar (Tóth et al. ACP 18, 10407–10418, 2018), and even their optical properties are known (Hoffer et al. ACP 16, 239–246, 2016). By using POT, I feel the definition of tar ball is diluted and thereby the utility of the term diminished. In summary, I believe it may be more prudent to call the POT particles just burning-related primary organics (PO), and it could be mentioned that the spherical ones appear to be tar balls. But, in the end, it is up to the authors what they wish to call these particles.

Response: We appreciated the referee's critical comments. We accepted the referee's suggestion, the term POT was removed and burning-related primary organic aerosol (POA) particles were used in the revised manuscript, especially, the spherical primary organic particles were called tar balls as suggested.

2. Optical properties. The calculations for coated absorbing organic particles are interesting but I do not completely understand Figure 10. (1) What is the explanation for the insensitivity of ACS enhancement to the Dp/Dc size ratios larger than about 1.5? (2) What is the reason for the apparently random variation of ACS enhancement with Dc? I wonder if any optical measurements were done under hazy conditions during the sampling campaign? If such results are available, it would be interesting to compare them with the models.

Response: It will be very helpful to compare the simulation results with optical measurements. Unfortunately, the optical parameters were not measured during this observation, otherwise we would be willing to compare for further verification. (1) In Figure 10 we show that the absorption enhancement strongly depends on the core diameter and very little on the D_p/D_c when $D_p/D_c>1.5$. Similar variation trends were also reported in other studies (e.g., Bond et al., *J. Geophys. Res.*, 111, D20211, 2006; Wu et al., *Atmos. Chem. Phys.*, 18, 289–309, 2018). The "lensing effect" of secondary aerosol coating could significantly enhance the absorption capacity of the light-absorbing core. The incident light that would not pass through the core can finally reach the core and be absorbed after the refraction and internal reflections by the coating, which hence increases the absorption cross sections. As has been

illustrated in detail in the previous paper (Fuller et al., *J. Geophys. Res.*, 104, 15941–15954, 1999), the absorption cross sections rise monotonically as the thickness of the coating increases until the dipole resonance of the coated particle (for example D_p/D_c=1.5 in this study) is reached. From there, the absorption cross sections oscillate more and more rapidly as higher-order particle resonances are encountered. (2) The ACS enhancement with D_c is not randomly varied. Enhancement is always greater than one—that is, coating always increases absorption, never decreases it; enhancement can be extremely high for small cores; and for larger cores enhancement is nearly constant. This phenomenon is introduced in detail in the previous paper which conducted the Mie calculations for the core-shell light-absorbing carbon particles (Bond et al., *J. Geophys. Res.*, 111, D20211, 2006).

Figure 1, showing the relationship among the absorption amplification (i.e., ACS enhancement in this study), core diameter, shell diameter, and D_p/D_c, was modified from this paper. It is clear that the small cores have very high enhancements; when the core size increases, the enhancement decreases largely and then after a certain core size the enhancement increases slowly but not beyond a certain value. Because the Mie calculations involve very complex electromagnetic theories and formulas, it is very hard to explain these results comprehensively. In this study, we used the results from the Mie calculation directly but do not go deep into the reasons for variations.

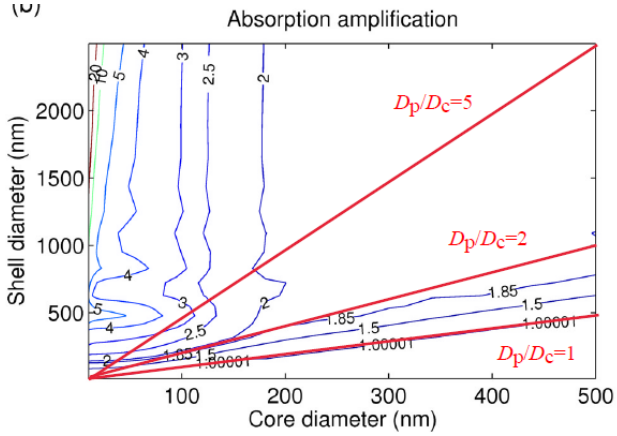

Figure 1. A contour plot of absorption amplification calculated by the concentric core-shell soot model at 550 nm. Assumptions: core m=1.85−0.71i and shell m=1.55−1.0^{-6}i. This graph is modified from Bond et al. (J. Geophys. Res., 111, D20211, 2006)

References:

Bond, T. C., Habib, G., and Bergstrom, R. W.: Limitations in the enhancement of

visible light absorption due to mixing state, J. Geophys. Res.-Atmos., 111, https://doi.org/10.1029/2006JD007315, 2006.

Wu, C., Wu, D., and Yu, J. Z.: Quantifying black carbon light absorption enhancement with a novel statistical approach, Atmos. Chem. Phys., 18, 289-309, 10.5194/acp-18-289-2018, 2018.

Fuller, K. A., Malm, W. C., and Kreidenweis, S. M.: Effects of mixing on extinction by carbonaceous particles, J. Geophys. Res.-Atmos., 104, 15941-15954, https://doi.org/10.1029/1998JD100069, 1999.

3. Size changes. If the particles were transported from the rural site to Beijing, and during transport secondary aerosol formed on them, it does not see logical that their sizes decreased. The explanation offered is that large particles deposited but this process does not seem feasible for the particles in this size range. Can you please provide some more discussion on this issue?

   Response: We are sorry for the puzzling problem. We should emphasize that the sizes of the whole aged particles indeed increased after the secondary aerosol formed on them as shown in Figure 7 in the manuscript. What we refer to is that the sizes of uncoated POA particles slightly decreased during the regional transport.

4. Line 29: "average particle-to-core ratios."- it is unclear what ratios; probably "diameter ratios" would be correct.

   Response: We corrected it as "average particle-to-core diameter ratios".

5. Line 32: replace "we using.." with "Using Mie theory we estimated.. "

   Response: Changed.

6. Line 61: chromatography

   Response: Corrected.

7. Line 64-66: subject of sentence unclear

   Response: We revised this sentence in the revised manuscript as follows:

   Line 65-67: Therefore, to document the aging processes of different particles in the NCP is of great significance for revealing the particle transformation in the atmosphere and better assessing the aerosol climatic effects.

8. Line 85: "properties" instead of "information"

   Response: Changed.

9. Line 178-179: "five grids.. were selected" - I guess "five grid meshes: : : were selected" would be correct.

   Response: Corrected.

10. Line 191: primary organic tar, POT: I do not understand the utility of this name and abbreviation. First, tar should be organic anyway, so "organic tar" is a tautology. Second, how do you know it is tar?

    Response: As answered in question 1, we accepted the referee's suggestion and replaced the term POT with the primary organic aerosol (POA) particles, and the spherical organic particles were called tar balls.

11. Line 195-197: Hoffer et al. ACP 16, 239–246, 2016 found 1.84 - 0.21i for tar balls - I wonder if this would make a large difference in your calculations, compared to the value by Alexander et al.

    Response: We further calculated the absorption cross section and enhancement factors through Mie calculation using the refractive index of 1.84−0.21*i*, the results are listed in the Table below. There is no big difference between the results acquired by using the two refractive indices 1.67−0.27*i* and 1.84−0.21*i*.

    Please see line 390-394:

    It should be noted that another RI of 1.84−0.21*i* for tarballs was reported by Hoffer et al. (2016). The average Mie calculation results at the GC rural and BJ urban sites obtained by the RIs of 1.67−0.27*i* (used in this study) and 1.84−0.21*i* were compared and we found that the two RIs only cause little differences between the results (Table S3). Therefore, only the results from the RI of 1.67−0.27*i* were used and discussed in this study.

Table S3. Comparison between the average Mie calculation results acquired by two reported refractive indices of 1.67−0.27*i* and 1.84−0.21*i* in previous studies.

Location	Pollution level	ACS_{actual}[a]	$ACS_{non\text{-}aging}$[b]	E_{abs}[c]	Refractive Index
Gucheng	Heavy (Early stage)	3.09	3.01	1.02	1.67−0.27*i* (Alexander et al., 2008)
	Heavy (Middle stage)	3.97	3.53	1.12	
	Heavy (Late stage)	4.43	3.18	1.39	
Beijing	Moderate	2.06	1.86	1.10	
	Heavy	3.00	2.15	1.39	
Gucheng	Heavy (Early stage)	3.08	3.00	1.02	1.84−0.21*i* (Hoffer et al., 2016)
	Heavy (Middle stage)	3.97	3.51	1.13	
	Heavy (Late stage)	4.47	3.13	1.43	
Beijing	Moderate	2.04	1.85	1.10	
	Heavy	2.99	2.14	1.40	

[a]ACS_{actual} represents the absorption cross section of individual POA-containing particles (including core–shell POA–SIA and bare POA) under the actual scenario;

[b]$ACS_{non\text{-}aging}$ represents the absorption cross section of individual uncoated POA particles

(including POA cores and bare POA) under the particle non-aging scenario;

[c]E_{abs} represents the absorption enhancement factor due to the particle aging, i.e., ratio of ACS_{actual} to $ACS_{non\text{-}aging}$.

References:

Alexander, D. T. L., Crozier, P. A., and Anderson, J. R.: Brown carbon spheres in East Asian outflow and their optical properties, Science, 321, 833-836, 2008.

Hoffer, A., Toth, A., Nyiro-Kosa, I., Posfai, M., Gelencser, A.: Light absorption properties of laboratory-generated tar ball particles, Atmos. Chem. Phys., 16, 239-246, 10.5194/acp-16-239-2016, 2016.

12. Line 246-249: unclear sentence, please reword

Response: We reworded this sentence in the revised manuscript as follows:

Line 247-250: Contrasting to the transition periods at two sampling sites, we found that the SIA concentration increased significantly, meanwhile, the OM concentration only slightly increased at the GC rural and BJ urban sites with the consistent decreasing WS and increasing RH during the heavily polluted period.

13. Line 266-267 and text that follows: "TEM observations show a distinct group of spherical and irregular primary organic particles.." - I think TEM observations indeed show the morphologies of the particles but they do not provide direct information on their "organic" nature (only their elemental composition), let alone their primary origin. Please try to distinguish observations from interpretation.

Response: Thanks for this comment. According to the referee's suggestion, these sentences were modified to avoid over interpretation in the description of the observation results.

14. Line 278: Could it be just PO?

Response: Accepted.

15. Line 295: "agrees" instead of "consists"

Response: Corrected.

16. Line 372: influences

Response: Corrected.

17. Line 376-377: how were the absorption cross sections estimated?

Response: We added more description about the model calculations in the method section 2.5. We think this will make the calculation results clearer.

Please see line 211-222:

After running the Mie calculation, the attenuation efficiency (Q_{atn}), scattering

efficiency (Q_{sca}), and absorption efficiency (Q_{abs}) of an individual particle were output with their definitions as follows (Aden and Kerker, 1951; Toon and Ackerman, 1981):

$$Q_{atn} = \left(\frac{2}{x^2}\right) \sum_{n=1}^{\infty} (2n+1)[\mathrm{Re}(a_n + b_n)] \quad (1)$$

$$Q_{sca} = \left(\frac{2}{x^2}\right) \sum_{n=1}^{\infty} (2n+1)(|a_n|^2 + |b_n|^2) \quad (2)$$

$$Q_{abs} = Q_{atn} - Q_{sca} \quad (3)$$

where $x = \frac{\pi D}{\lambda}$, is the dimensionless size parameter of the particle diameter D and the wavelength of light λ; a_n and b_n are calculated from Riccati–Bessel functions of the particles sizes and refractive indices (Bohren and Huffman, 1983); The symbol Re denotes the real part of the complex quantity a_n+b_n. The ACS of a particle can be obtained via multiplying the Q_{abs} by the geometric cross section of the particle as follows:

$$\mathrm{ACS} = Q_{abs} \times \frac{\pi D^2}{4} \quad (4)$$

References:

Aden, A. L., and Kerker, M.: Scattering of Electromagnetic Waves from Two Concentric Spheres, J.Appl. Phys., 22, 1242-1246, 10.1063/1.1699834, 1951.

Toon, O. B., and Ackerman, T. P.: Algorithms for the calculation of scattering by stratified spheres, Appl. Opt., 20, 3657-3660, 10.1364/ao.20.003657, 1981.

Bohren, C. F., and Huffman, D. R.: Absorption and scattering of light by small particles, John Wiley & Sons, New York, 1983.

18. Line 405-409: this seems important, but I do not understand the statement completely.

Response: We are sorry for the puzzling issue. After consideration we decided to delete this sentence.

Persistent residential burning-related primary organic particles during wintertime hazes in North China: insights into their aging and optical changes

Lei Liu[1], Jian Zhang[1], Yinxiao Zhang[1], Yuanyuan Wang[1], Liang Xu[1], Qi Yuan[1], Dantong Liu[1], Yele Sun[2], Pingqing Fu[3], Zongbo Shi[4], and Weijun Li[1,*]

[1]Department of Atmospheric Sciences, School of Earth Sciences, Zhejiang University, Hangzhou 310027, China

[2]State Key Laboratory of Atmospheric Boundary Layer Physics and Atmospheric Chemistry, Institute of Atmospheric Physics, Chinese Academy of Sciences, Beijing 100029, China

[3]Institute of Surface-Earth System Science, Tianjin University, Tianjin 300072, China

[4]School of Geography, Earth and Environmental Sciences, University of Birmingham, Birmingham B15 2TT, UK

Correspondence to: Weijun Li (liweijun@zju.edu.cn)

Abstract

Primary organic aerosol (POA) is a major component of $PM_{2.5}$ in winter polluted air in the North China Plain (NCP), but our understanding on the atmospheric aging process of POA particles and the resulting influences on their optical properties is limited. As part of the Atmospheric Pollution and Human Health in a Chinese Megacity (APHH-Beijing) programme, we collected airborne particles at an urban site (Beijing) and an upwind rural site (Gucheng, Hebei province) in the NCP during 13–27 Nov. 2016 for microscopic analyses. We confirmed that large amounts of light-absorbing spherical POA (i.e., tarball) and irregular POA particles with high viscosity were emitted from the domestic coal and biomass burning at the rural site and were further transported to the urban site during regional wintertime hazes. During the heavily polluted period ($PM_{2.5}$ > 200 μg m^{-3}), more than 60% of these burning-related POA particles were thickly coated with secondary inorganic aerosols (named as core–shell POA–SIA particle) through the aging process, suggesting that POA particles can provide surfaces for the heterogeneous reactions of SO_2 and NO_x. As a result, their average particle-to-core diameter ratios at the rural and urban sites in the heavily polluted period increased to 1.60 and 1.67, respectively. Interestingly, we found that the aging process did not change the morphology and sizes of POA cores, indicating that these POA particles are quite inert in the atmosphere and can be transported long distances. Using Mie theory we estimated that the absorption capacity of POA particles was enhanced by ~1.39 times in the heavily polluted period at the rural and urban sites due to the "lensing effect" of secondary inorganic coatings. We highlight that the "lensing effect" on burning-related POA particles should be considered in radiative forcing models and the governments should continue to promote clean energy in rural areas to effectively reduce primary emissions.

1 Introduction

Atmospheric aerosol particles can affect regional and global energy budgets by scattering or absorbing solar radiation, modify microphysical properties of clouds by acting as cloud condensation nuclei (CCN), and exert adverse effects on human health such as respiratory and cardiovascular diseases (IPCC, 2013; West et al., 2016). With rapid industrialization and urbanization in past decades, severe air pollution characterized by high concentrations of fine particulate matter ($PM_{2.5}$) frequently occurs in China, especially the regional hazes in the North China Plain (NCP), which has received wide concerns from the public, governments, and scientists (Sun et al., 2016). Many previous studies have shown that synergetic effects from extensive emissions of primary particles and gaseous precursors, efficient secondary aerosol formation, regional transport, and unfavorable meteorological conditions are main factors contributing to haze formation in the NCP (Chang et al., 2018; Liu et al., 2016; Zhong et al., 2019). In particular, long-term measurements have confirmed that wintertime haze episodes in Beijing are commonly initiated by regional transport of air pollutants from the south parts of NCP (e.g., Hebei and Henan provinces) under weak southerly winds and then evolved through the massive secondary aerosol formation via heterogeneous reactions (Ma et al., 2017; Sun et al., 2014; Zheng et al., 2015).

During the regional transport and evolution of haze episodes, complex physical and chemical processes in the atmosphere, such as condensation, coagulation, and heterogeneous reactions, could largely alter the morphology, composition, size, and mixing state of individual particles, which is also known as "particle aging" (Li et al., 2016a). Particle aging could further influence the optical property, health effects, hygroscopicity, and CCN activity of aerosol particles, although different types of particles might have different impacts (Fan et al., 2020; Li et al., 2016b; Riemer et al., 2019). Up to now, most of the studies conducted in the NCP mainly applied various bulk online and offline aerosol analytical techniques (e.g., online aerosol mass spectrometry (AMS) and offline ion chromatography (IC)) to explore mass concentrations, possible sources, and formation mechanisms of different aerosol

components, such as sulfate, nitrate, and organic aerosols (Chen et al., 2020; Cheng et al., 2016; J. Li et al., 2020; Sun et al., 2016; Wang et al., 2020). However, knowledge on the aging process of aerosol particles remains limited. Therefore, further to document the aging processes of different particles in the NCP through microscopic individual particle analysis is of great significance for revealing the particle transformation in the atmosphere and better assessing the aerosol climatic effects (Du et al., 2019; Li et al., 2016a).

Field observations have shown that carbonaceous aerosols, including organic aerosol (OA) and black carbon (BC), are the dominant components of $PM_{2.5}$ during heating seasons in the NCP, which accounts for more than 50% of the total $PM_{2.5}$ (Liu et al., 2020; P. Liu et al., 2017; Zhang et al., 2020). Source apportionment results reveal that residential coal and biomass burning in rural areas are the major contributors to the carbonaceous aerosols during wintertime hazes in the NCP (Li et al., 2017). BC is the major light-absorbing aerosol in the atmosphere, which can strongly absorb solar radiation and thus affect the regional and global climate (Bond et al., 2013; D. Liu et al., 2017; Wang et al., 2014). In recent years, a bunch of studies have well documented the aging process of BC particles and revealed that the secondary inorganic and organic coatings (e.g., sulfate and organics) can significantly enhance the light absorption capacity of the internally mixed BC particles via the "lensing effect" (Chakrabarty and Heinson, 2018; Wang et al., 2017). Recently, light-absorbing organic aerosols, also known as brown carbon (BrC), have been reported to be ubiquitous in the atmosphere in the NCP (Wang et al., 2018; Xie et al., 2019). Many studies have demonstrated that primary OA (POA) emitted from residential coal and biomass burning is the major source of BrC, and the chemical composition and optical properties of BrC in freshly emitted POA as well as the BrC in the ambient atmosphere were analyzed in detail using bulk techniques such as mass spectrometry and UV–visible spectrophotometry (M. Li et al., 2019; X. Li et al., 2020; Song et al., 2018; Sun et al., 2017; Yan et al., 2017). However, only a few studies characterized microscopic properties such as the morphology and mixing state of fresh burning-related POA particles by

transmission electron microscopy (TEM) (L. Liu et al., 2017; Zhang et al., 2018). The abundance and aging process of burning-related POA particles in the atmosphere and the resulting influences on their optical properties remain unknown in the NCP.

This study, as part of the Atmospheric Pollution and Human Health in a Chinese Megacity (APHH-Beijing) programme (Shi et al., 2019), aims to explore the atmospheric aging process of POA particles emitted from the residential coal and biomass burning in rural areas following the regional transport and evolution of haze episodes. Individual particle samples were collected in urban Beijing and the surrounding rural regions during the winter campaign and then were analyzed by microscopic methods to obtain the morphology, composition, size, and mixing state of different individual particle types. Besides, bulk analyses of aerosol chemical composition were also conducted to help understand the evolution of haze episodes. We found that large amounts of POA particles were emitted from the domestic coal and biomass burning in winter in the NCP. For the first time, we characterized the aging process of such burning-related POA particles based on microscopic analyses and Mie theory was used to further explore the resulting influences on their optical properties.

2 Experimental methods

2.1 Sampling sites and sample collections

Field observations were carried out simultaneously at the Beijing (BJ) urban site (39°58'27" N, 116°22'16" E) and Gucheng (GC) rural site (39°08'58" N, 115°44'00" E) during 13–27 Nov. 2016. Locations of two sampling sites in the NCP are displayed in Fig. 1a. The BJ urban site, located on the rooftop of a two-story building (8 m above ground level (a.g.l.)) in the Tower Division of the Institute of Atmospheric Physics, Chinese Academy of Sciences, is between the north 3rd and 4th ring roads and surrounded by commercial area and residential apartments (Fig. 1b). The GC rural site, located on the rooftop of a three-story building (12 m a.g.l.) at the Gucheng Integrated Ecological–Meteorological Observation and Experimental Station of the Chinese Academy of Meteorological Sciences in Dingxing county, Hebei province, is 120 km to the southwest of the BJ urban site and

surrounded by many villages and farmlands (Fig. 1c). The detailed information about the two sampling sites can be found in the introduction paper of APHH-Beijing programme (Shi et al., 2019). The 24-h backward trajectories of air masses ending at the height of 100 m (a.g.l.) over the BJ urban site (Fig. 1a) were calculated using the NOAA Air Resources Laboratory's HYbrid Single-Particle Lagrangian Integrated Trajectory (HYSPLIT) model (Stein et al., 2016).

At the BJ urban site, the species in non-refractory submicron aerosols (NR-PM_1) including organic matter (OM), SO_4^{2-}, NO_3^-, NH_4^+, and Cl^- were measured by a high-resolution aerosol mass spectrometer (HR-AMS, Aerodyne Inc., USA). At the GC rural site, $PM_{2.5}$ samples were collected twice a day during the daytime (8:00 to 20:00) and nighttime (20:00 to 8:00 the next day) onto 90 mm-diameter quartz filters (Pallflex 7204, Pall Corporation, USA) using a medium-volume sampler (TH-150A, Wuhan Tianhong Instruments Co., Ltd., China) at a flow rate of 100 L min^{-1}. Field blank samples were collected for approximately 15 min without starting the sampler. The filters were prebaked at 450°C for 6 h before sampling to remove any possible contaminants. All the collected samples were sealed individually in aluminum foil bags and stored in a refrigerator at −20 °C for further analyses.

Individual particle samples were collected onto copper (Cu) TEM grids coated by formvar and carbon films (carbon type-B, 300 mesh, Beijing XXBR Technology Co., Ltd., China) at the GC rural and BJ urban sites using an individual particle sampler (DKL-2, Qingdao Genstar Electronic Technology Co., Ltd., China) at a flow rate of 1 L min^{-1}. The DKL-2 sampler consists of a single-stage impactor with a 0.5 mm-diameter jet nozzle. Sampling duration ranged from 8 s to 3 min depending on the pollution levels to avoid overlap of particles on the TEM grids. Individual particle samples were placed in a clean and airtight container with controlled temperature (*T*, 25±1°C) and relative humidity (RH, 20±3%) for further analyses. The detailed information about the individual particle samples collected at the two sites is listed in Table S1.

Meteorological parameters including *T*, pressure (*P*), RH, wind speed (WS), and wind direction

(WD) were recorded every 5 min at two sampling sites using a pocket weather station (Kestrel 5500, Nielsen-Kellermann Inc., USA). The hourly concentrations of $PM_{2.5}$ and gaseous pollutants (i.e., SO_2, NO_2, CO, and O_3) during the sampling period at two monitoring stations (i.e., Dingxing government station: 39°15'42" N, 115°48'06" E; Beijing Olympic center station: 40°00'11" N, 116°24'25" E) close to GC rural and BJ urban sites were downloaded from the website of air quality online monitoring and analysis platform (https://www.aqistudy.cn/). All the data in this study are presented at the Beijing local time (UTC+8).

2.2 $PM_{2.5}$ chemical analysis

$PM_{2.5}$ samples collected at the GC rural site were analyzed to obtain their water-soluble inorganic ions (WSIIs), organic carbon (OC), and elemental carbon (EC). For the analysis of WSIIs, two16 mm-diameter punches from each $PM_{2.5}$ sample were put into a vial, followed by adding 20 mL deionized water (18.2 MΩ). Then these vials were placed in an ultrasonic water bath for 30 min to extract WSIIs. The solutions were further filtered using PTFE syringe filters with 0.45 μm pore size to remove insoluble components and then analyzed by an ion chromatography system (Dionex ICS 600, ThermoFisher Scientific, USA). Finally, concentrations of three anions (Cl^-, SO_4^{2-}, and NO_3^-) and five cations (Na^+, NH_4^+, K^+, Mg^{2+}, and Ca^{2+}) were obtained. Concentrations of OC and EC in $PM_{2.5}$ samples were determined by analyzing a 1×1.5 cm^2 punch from each filter with an OCEC analyzer (Model 5L, Sunset Laboratory Inc. USA), which adopted the NIOSH870 temperature protocol with thermal–optical transmittance for charring correction. The OM concentration was estimated via multiplying OC concentration by a factor of 1.6, based on the previous studies (Xing et al., 2013; Zheng et al., 2015).

2.3 AMS data analysis

The HR-AMS V-mode data were analyzed using standard data analysis software (PIKA V1.56D). A constant collection efficiency (CE) of 0.5, similar to the previous study conducted in winter at the BJ site (Sun et al., 2014), was applied to the HR-AMS datasets to obtain mass concentrations of NR-

PM_1 species. The relative ionization efficiencies used for OM, SO_4^{2-}, NO_3^-, NH_4^+, and Cl^- were 1.4, 1.2, 1.1, 5.0, and 1.3, respectively. Positive matrix factorization (PMF) is a receptor model to identify potential sources without local source profiles provided (Xu et al., 2020). PMF was performed on the high-resolution mass spectra of organics measured by HR-AMS. Six OA factors were identified including fossil fuel-related OA (FFOA), cooking OA (COA), biomass burning OA (BBOA), oxidized primary OA (OPOA), oxygenated OA (OOA), and aqueous-phase OOA (aqOOA). Detailed information on the processing of HR-AMS data can be found in the related paper during the same campaign (Xu et al., 2019).

2.4 Individual particle analysis

Individual particle samples were analyzed using TEM (JEM-2100, JEOL Ltd., Japan) operated at a 200 kV accelerating voltage to acquire morphology and sizes of individual particles and mixing state (i.e., internally or externally mixed) of different aerosol components within one individual particle. TEM is equipped with an energy-dispersive X-ray spectrometer (EDS, INCA X-Max^N 80T, Oxford Instruments, UK) to semi-quantitatively detect the elemental composition of individual particles with atomic number greater than six ($Z \geq 6$). It should be noted that Cu peaks in the EDS spectra are not considered due to the interference from the Cu substrate of TEM grids. The distribution of aerosol particles on TEM grids is not uniform, with particle size decreasing from the center to the edge of distribution area. Therefore, to ensure the analyzed particles are representative, five grid meshes from the center to the edge of particle distribution area in each sample were selected to conduct TEM analysis. TEM images were manually processed by the RADIUS 2.0 software (EMSIS GmbH, Germany) to determine the particle types, areas, perimeters, and equivalent circle diameters (ECD). After a labor-intensive operation, a total of 1197 particles at the BJ urban site and 2443 particles at the GC rural site were analyzed.

Scanning electron microscope (SEM, Ultra 55, Carl Zeiss Microscopy GmbH, Germany) was operated at the 10 kV accelerating voltage and secondary electron (SE2) mode to observe the particle

surface topography. Furthermore, particles were imaged at a tilt angle of 75° to realize the visualization of their morphology in the vertical dimension.

2.5 Optical property calculation

Mie theory has been widely used to calculate the optical properties of individual particles by assuming a spherical core–shell structure (Chylek et al., 2019; Wu et al., 2018; Yu et al., 2019). In this study, the light absorption cross sections (ACS) of internally mixed POA particles with secondary inorganic aerosol (SIA) shell (named as core–shell POA–SIA particle), as well as the POA cores and bare POA particles at the wavelength of 550 nm were calculated with BHCOAT Mie code (Bohren and Huffman, 1983). Details for the classification of POA and POA–SIA particles, please refer to Section 3.2. For the core–shell POA–SIA particles, a refractive index (RI) of 1.55−0i for non-light-absorbing SIA coating (Denjean et al., 2014) and 1.67−0.27i for light-absorbing POA core (Alexander et al., 2008) were adopted at the wavelength of 550 nm; and the ECD of each POA–SIA particle and its POA core obtained from the TEM images were used respectively as the input particle diameter (D_p) and core diameter (D_c) in the Mie calculation, which made the calculation sufficient to approximate reality. Because a core–shell structure is considered in the Mie model (Bond et al., 2006), for the uncoated POA particles (including POA cores without SIA shell and bare POA particles), the ECD of each POA particle and one-tenth of it were input as the D_p and D_c, respectively. Then in the case of vanishing the refractive index difference between the shell and core (i.e., POA core and POA shell, RI=1.67–0.27i), the Mie model can be applied to homogeneous particles. Besides, we also constructed models of core–shell POA–SIA particles with different POA core diameters (i.e., D_c=100, 200, 300, 400, 500, 700, 900, 1100, 1300, and 1500 nm) and particle-to-core diameter ratios (i.e., D_p/D_c ranged from 1 to 6 with an interval of 0.1), and calculated their ACS to further explore the effects of D_c and D_p/D_c changes on the light absorption enhancement factors (E_{abs}) of POA particles.

After running the Mie calculation, attenuation efficiency (Q_{atn}), scattering efficiency (Q_{sca}), and absorption efficiency (Q_{abs}) of an individual particle were output with their definitions as follows

(Aden and Kerker, 1951; Toon and Ackerman, 1981):

$$Q_{atn} = \left(\frac{2}{x^2}\right) \sum_{n=1}^{\infty} (2n+1)[\mathrm{Re}(a_n+b_n)] \quad (1)$$

$$Q_{sca} = \left(\frac{2}{x^2}\right) \sum_{n=1}^{\infty} (2n+1)(|a_n|^2+|b_n|^2) \quad (2)$$

$$Q_{abs} = Q_{atn} - Q_{sca} \quad (3)$$

where $x = \frac{\pi D}{\lambda}$, is the dimensionless size parameter of the particle diameter D and the wavelength of incident light λ; a_n and b_n are calculated from Riccati–Bessel functions of the particle sizes and refractive indices (Bohren and Huffman, 1983); The symbol Re denotes the real part of the complex quantity a_n+b_n. The ACS of a particle can be obtained via multiplying the Q_{abs} by geometric cross section of the particle shown as follow:

$$\mathrm{ACS} = Q_{abs} \times \frac{\pi D^2}{4} \quad (4)$$

3 Results and Discussion

3.1 Overview of a regional haze episode

A typical regional heavy haze episode in the NCP was observed at the GC rural and BJ urban sites during 22–27 Nov. 2016. Based on variations of hourly $PM_{2.5}$ concentrations, three pollution levels are defined: clean ($PM_{2.5} \leq 75$ μg m^{-3}), moderate pollution (75 μg m^{-3} < $PM_{2.5} \leq 200$ μg m^{-3}), and heavy pollution ($PM_{2.5} > 200$ μg m^{-3}). According to the above criteria, we classified clean period (21 Nov. 0:00 to 22 Nov. 19:00) and heavily polluted period (22 Nov. 20:00 to 27 Nov. 10:00) at the GC rural site; clean period (21 Nov. 0:00 to 24 Nov. 9:00), moderately polluted period (24 Nov. 10:00 to 25 Nov. 16:00), and heavily polluted period (25 Nov. 17:00 to 27 Nov. 2:00) at the BJ urban site (Fig. 2). Furthermore, we divided the heavily polluted period at the GC rural site into the early stage (22 Nov. 20:00 to 23 Nov. 20:00), middle stage (23 Nov. 20:00 to 24 Nov. 20:00), and late stage (24 Nov. 20:00 to 27 Nov. 8:00) based on the evolution of chemical species in $PM_{2.5}$ (Fig. 2a). The average

meteorological parameters and mass concentrations of $PM_{2.5}$, aerosol chemical species, OA factors, and gaseous pollutants in different periods at two sampling sites are summarized in Table S2.

Strong northwesterly winds (> 4 m s^{-1}) accompanied with rain and snow invaded the NCP during 20−21 Nov. (Fig. S1), leading to fast dispersion of air pollutants (Figs. 2 and S2). The low T (−8 to 5°C) and WS (< 2 m s^{-1}) were displayed after the cold front (Fig. S1), which can facilitate the accumulation of air pollutants (Zhong et al., 2019). At the GC rural site, $PM_{2.5}$ concentration began to increase at 18:00 on 22 Nov. and quickly reached a peak of 394 μg m^{-3} within six hours (Fig. 2a). $PM_{2.5}$ chemical analysis reveals that OM (252.8 μg m^{-3}) accounted for 83% of the $PM_{2.5}$ in the nighttime sample on 22 Nov. (i.e., 22 Nov. 20:00 to 23 Nov. 8:00), causing the fast transition from the clean to heavily polluted period directly (Figs. 2a and S3a). In the early stage of heavily polluted period, the average $PM_{2.5}$ concentration (288.3 μg m^{-3}) increased by a factor of seven compared with that (39.8 μg m^{-3}) in the clean period, with OM being the largest contributor (185.1 μg m^{-3}) followed by SIA (i.e., sum of SO_4^{2-}, NO_3^-, and NH_4^+; 36.4 μg m^{-3}) (Table S2). At the BJ urban site, the air quality remained clean before 24 Nov. under continuous northerly winds (Figs. 2b and S1b). With prevailing winds changing from northerly to southerly on 24 Nov. (Fig. S1), polluted air parcels in the south of NCP were transported to Beijing (Fig. 1a), which has also been confirmed by another study conducted in the APHH-Beijing winter campaign (Du et al., 2019). Thus, the concentrations of $PM_{2.5}$, chemical species in NR-PM_1, CO, and SO_2 at the BJ urban site increased simultaneously and sharply from 09:00 on 24 Nov., causing the transition from the clean period to the moderately polluted period (Figs. 2b and S2b). The average $PM_{2.5}$ concentration in the moderately polluted period was 111.0 μg m^{-3}, 10 times higher than that (10.8 μg m^{-3}) in the clean period, and the OM and SIA contributed equally in NR-PM_1 with their average concentrations being 44.4 and 43.4 μg m^{-3}, respectively (Table S2). Following the haze evolution, $PM_{2.5}$ levels increased gradually to 312.3 and 396.8 μg m^{-3} in the middle and late stages of heavily polluted period at the GC rural site and to 281.0 μg m^{-3} in the heavily polluted period at the BJ urban site (Fig. 2 and Table S2). Contrasting to the

transition periods at two sampling sites, we found that the SIA concentration increased significantly, meanwhile, the OM concentration only slightly increased at the GC rural and BJ urban sites with the consistent decreasing WS and increasing RH during the heavily polluted period (Figs. 2 and S1). In a word, we observed that the SIA fraction in fine particles increased and the OM fraction decreased following the haze evolution (Fig. S3).

The concentrations and fractions of OM and EC at nighttime were much higher than those at daytime during the whole haze episode at the GC rural site (Figs. 2a and S3a), suggesting the continuous strong local combustion emissions at nighttime. Furthermore, the concentration of Cl^- (8–22 μg m^{-3}) was much higher than that of K^+ (1–3 μg m^{-3}) (Fig. 2a), which suggests more contributions from coal combustion than biomass burning at the GC rural site (Sun et al., 2014; Zhang et al., 2020). Based on the field investigation and $PM_{2.5}$ analysis, we concluded that the explosive increase of $PM_{2.5}$ at the GC rural site was initiated by strong local emissions and accumulation of POA from residential coal combustion for heating and a small fraction of biomass burning for cooking in rural areas. The PMF analysis shows that FFOA and BBOA (14.6–30.6 μg m^{-3}) contributed significantly (> 30%) to OM in the polluted period at the BJ urban site (Fig. S4 and Table S2), suggesting that POA emitted in rural areas were transported to Beijing under southerly winds. In summary, bulk analyses show that POA from residential coal and biomass burning consistently contributed to the regional haze, and SIA produced from the secondary formation had an increasing contribution at higher RH following the haze evolution.

3.2 Classification of individual particle types

In this study, TEM observations show abundant spherical and irregular particles comprised of C, O, and Si elements during this haze episode (Fig. 3a). These particles are stable under strong electron beams and appear as dark features in TEM images, reflecting their high thickness and refractory properties (Ebert et al., 2016; Liu et al., 2018). The SEM image acquired at a 75° tilt angle shows that these particles did not deform upon impaction and retained high vertical dimensions (Fig. 4),

284 indicating that these particles are in a solid state with high viscosity (Reid et al., 2018; Wang et al.,
285 2016). By contrast, the secondary particles (i.e., SIA and organic coating) became flat on the substrate
286 (Fig. 4). Previous studies have confirmed that these solid spherical and irregular particles are POA
287 particels emitted from coal and biomass burning (L. Liu et al., 2017; Zhang et al., 2018), especially
288 the spherical POA particles shown in Fig. 3a-1 are defined as tarballs containing light-absorbing BrC
289 (Adachi et al., 2019; C. Li et al., 2019; Pósfai et al., 2003; Zhang et al., 2018). The tarballs (Fig. 3a-
290 1) and irregular POA particles (Fig. 3a-2) are both burning-related POA particles and have similar
291 chemical composition and physical characteristics under the TEM despite their different shapes, thus
292 in this study we consider that irregular POA particles also contain light-absorbing BrC like tarballs.
293 Other typical individual particle types, such as SIA (Fig. 3b), mineral (Fig. 3c), soot (Fig. 3d),
294 and fly ash/metal (Fig. 3e) particles were also classified during this haze episode. The detailed
295 classification criteria of these particle types derived from the TEM images and their sources can be
296 found in our previous paper (Li et al., 2016a). It should be noted that some SIA particles were coated
297 with secondary organic coatings (Fig. 3b) which were produced from the chemical oxidation of
298 volatile organic compounds (Li et al., 2016b). TEM observations further show the internal mixture of
299 POA or soot particles with SIA, i.e., POA–SIA (Fig. 3f) and soot–SIA (Fig. 3g). To better understand
300 number variations of different particle types, we classified the bare POA and POA–SIA particles as
301 the POA-containing particles, and bare soot and soot–SIA particles as soot-containing particles.

302 **3.3 Relative abundance of individual particle types**

303 Figure 5 shows number fractions of different particle types in different periods at GC rural and
304 BJ urban sites. At the GC rural site, POA-containing and soot-containing particles were the major
305 particle types with their corresponding contributions being 37.6% and 35.9% by number, followed
306 by SIA particles (22.4%) in the clean period. When the haze episode occurred at the GC rural site,
307 POA-containing particles became dominant in the early stage of heavily polluted period and its
308 number fraction (64.8%) was nearly twice that (37.6%) in the clean period (Fig. 5a). This result agrees

well with the bulk $PM_{2.5}$ analysis which shows a sharp increase in OM concentration in the early stage of heavily polluted period (Fig. 2a). With increasing pollution levels from the early stage to the late stage of heavily polluted period, the fraction of POA-containing particles slightly decreased from 64.8% to 50.8%, by contrast, the fraction of SIA particles increased from 4.6% to 12.4% (Fig. 5a). The variations of POA-containing and SIA particles are similar to the results from the bulk $PM_{2.5}$ analysis as shown in Fig. 2a.

At the BJ urban site, the contribution of POA-containing particles (15.1%) in the clean period was much lower than that (37.6%) at the GC rural site (Fig. 5). Following the transition from the clean period to the moderately polluted period at the BJ urban site, the fraction of POA-containing particles (66.2%) increased significantly by more than a factor of four compared with that (15.1%) in the clean period. Meanwhile, fractions of soot-containing, mineral, and SIA particles decreased largely. When the pollution level changed to the heavily polluted period, similar to the situation at the GC rural site, the fraction of SIA particles increased from 7.8% to 13.2% and the fraction of POA-containing particles decreased slightly from 66.2% to 52.8% (Fig. 5b). Overall, the individual particle analysis results consist well with changes in aerosol chemical components obtained by the bulk analysis as shown in Fig. 2. Furthermore, individual particle analysis reveals that POA-containing particles dominated (> 50% by number) in the rural and urban air during the regional wintertime haze episode.

3.4 Atmospheric aging of POA particles

TEM images clearly show the morphology and mixing state of individual particles in different polluted periods at GC rural and BJ urban sites (Fig. 6). At the GC rural site, we found that large amounts of bare POA particles, especially tarballs occurred in the early stage of heavily polluted period (Fig. 6a). Based on the integrated analyses of individual particles and bulk samples, we confirmed that POA particles emitted from the intense domestic coal and biomass burning for heating and cooking contributed significantly to the deterioration of air quality in rural areas. When the haze

episode evolved into the late stage of heavily polluted period, we found that most of the POA particles were coated with SIA (i.e., POA–SIA particle) forming the core–shell structure (Fig. 6b). This result indicates that POA particles in the regional haze layer provided surfaces for the heterogeneous reactions of SO_2 and NO_x, which promotes the formation of SIA on POA particles in the humid polluted air (Ebert et al., 2016; Zhang et al., 2017).

Following the regional transport of polluted air masses from the south to the north of the NCP, abundant POA particles occurred in the moderately polluted period at the BJ urban site (Fig. 6c). Therefore, we conclude that the POA particles emitted in the rural areas in the south of the NCP could be transported to the BJ urban site and significantly affect the urban air quality. Following the haze evolution, similar to those at the GC rural site, the POA particles aged and became core–shell POA–SIA particles at the BJ urban site in the heavily polluted period (Fig. 6d).

Based on the mixing state of POA-containing particles, we found that following evolution of the haze episode, the fraction of bare POA particles was reduced by twice from 91.4% in the early stage to 39.6% in the late stage of heavily polluted period at the GC rural site, and the fraction of POA–SIA particles correspondingly increased by seven times from 8.6% to 60.4% (pie charts in Fig. 7). Similarly, at the BJ urban site, the fraction of bare POA particles decreased from 70.4% in the moderately polluted period to 31.4% in the heavily polluted period, and the fraction of POA–SIA particles increased correspondingly from 29.6% to 68.6% (pie charts in Fig. 7). Consequently, the average size of POA-containing particles increased from 505 nm in the early stage to 837 nm in the late stage of heavily polluted period at the GC rural site and from 443 nm in the moderately polluted period to 732 nm in the heavily polluted period at the BJ urban site (Fig. 7a). Interestingly, the average sizes of uncoated POA particles (i.e., POA cores and bare POA) remained similar following the haze evolution, with their respective values being 469, 508, and 465 nm in the early, middle, and late stages of heavily polluted period at the GC rural site and 381 and 379 nm in the moderately and heavily polluted periods at the BJ urban site (Fig. 7b). The average sizes of uncoated POA particles at the BJ

359 urban site were slightly smaller than those at the GC rural site, which is reasonable because the fresh
360 POA particles with larger sizes could be collected at the GC rural site close to emission sources and
361 larger ones are more likely to be removed during the regional transport (Seinfeld and Pandis, 2006).
362 Adachi et al. (2018) reported that tarballs retained their spherical shapes and the particle masses and
363 sizes did not change largely when heated to 300°C in TEM. As a result, we conclude that the POA
364 particles should be quite physically stable and chemically inert in the atmosphere, which can be
365 transported over long distances.

366 The D_p/D_c ratio can be used to indicate the aging degree of POA-containing particles in the
367 atmosphere (Chen et al., 2017; Li et al., 2011). By calculating the D_p/D_c ratio, we realized
368 quantification of the aging degree of POA-containing particles as shown in Fig. 8. In the early stage
369 of heavily polluted period at the GC rural site, the POA-containing particles were mainly fresh bare
370 POA particles with a fraction of 91.4% (Fig. 7), therefore, the average D_p/D_c ratio was close to one
371 (1.02). Following the haze evolution at the GC rural and BJ urban sites, average D_p/D_c ratios increased
372 from 1.08 in the middle stage to 1.60 in the late stage of heavily polluted period at the GC rural site,
373 and from 1.11 in the moderately polluted period to 1.67 in the heavily polluted period at the BJ urban
374 site. The results indicate that POA particles were thickly coated with SIA due to the particle aging
375 process. Here we can obtain two conclusions based on the individual particle analysis: (1) more POA
376 particles continuously aged and were coated with SIA following the haze evolution; (2) the SIA
377 coating gradually grew through the heterogeneous conversion of gaseous precursors (e.g., SO_2 and
378 NO_x) in the polluted air. Therefore, the aging process of individual POA particles in wintertime hazes
379 well reflects the regional haze evolution in the NCP.

380 **3.5 Changes in light absorption of POA particles**

381 It is well known that organic aerosols emitted from coal and biomass burning are the main source
382 of light-absorbing BrC (M. Li et al., 2019; Lin et al., 2016; Sun et al., 2017). Recently, some
383 observation and modeling works show that BrC in haze layers over the NCP can affect the regional

energy budget (Feng et al., 2013; Wang et al., 2018; Xie et al., 2019). However, there is no answer on how the aging process of burning-related light-absorbing POA particles influences their optical absorption in the regional haze. Here using Mie theory we further explored variations in the optical absorption of individual POA particles following the haze evolution at the GC rural and BJ urban sites (Fig. 9). It should be noted that another RI of 1.84−0.21*i* for tarballs was reported by Hoffer et al. (2016). The average Mie calculation results at the GC rural and BJ urban sites obtained by the RIs of 1.67−0.27*i* (used in this sduty) and 1.84−0.21*i* were compared and we found that the two RIs only cause little differences between the results (Table S3). Therefore, only the results from the RI of 1.67−0.27*i* were used and discussed in this study.

At the GC rural site, the average ACS of individual POA-containing particles under the actual scenario (ACS_{actual}) in the early, middle, and late stages of heavily polluted period were estimated to be 3.09×10^{-14}, 3.97×10^{-14}, and 4.43×10^{-14} m^2, respectively (Fig. 9a). If all the POA-containing particles were not coated with SIA in each period (i.e., particle non-aging scenario), the corresponding average ACS of individual uncoated POA particles ($ACS_{non\text{-}aging}$) were 3.01×10^{-14}, 3.53×10^{-14}, and 3.18×10^{-14} m^2, respectively (Fig. 9a). Therefore, we obtained that the E_{abs} (i.e., ratio of ACS_{actual} to $ACS_{non\text{-}aging}$) were 1.02, 1.12, and 1.39 in the early, middle, and late stages of heavily polluted period, respectively, at the GC rural site (Fig. 9a). Similarly, at the BJ urban site, the E_{abs} were 1.10 and 1.39 in the moderately and heavily polluted periods, respectively, with the corresponding average ACS_{actual} being 2.06×10^{-14} and 3.00×10^{-14} m^2 and $ACS_{non\text{-}aging}$ being 1.86×10^{-14} and 2.15×10^{-14} m^2 (Fig. 9b). The light absorption capacity of individual POA particles at the BJ urban site was a little lower than that at the GC rural site (Fig. 9), which was mainly attributed to the smaller sizes of POA particles at the BJ urban site (Fig. 7).

To better understand the influence of SIA-coating thickness and POA-core diameter on the light absorption of POA–SIA particles, we modeled the variations in E_{abs} of POA–SIA particles (i.e., ratio of $ACS_{POA\text{–}SIA}$ to $ACS_{POA\ core}$) with different D_c as a function of D_p/D_c ratios (Fig. 10). Results show

409 that E_{abs} is sensitive to the changes in both D_c and D_p/D_c ratio. When $D_p/D_c < 1.5$, the E_{abs} increases
410 sharply with the increase of D_p/D_c ratio for different POA core sizes; but when $D_p/D_c > 1.5$, the E_{abs}
411 does not show an increase any more for particles with $D_c > 200$ nm, and the E_{abs} is limited to between
412 1.5 and 2 for particles with D_c ranging from 200 to 1500 nm (Fig. 10). The diameters of observed
413 POA cores at GC rural and BJ urban sites in this study were mainly in the range of 200 to 800 nm
414 (Fig. 7), thus the E_{abs} of observed POA–SIA particles in the NCP were mostly below 1.75 (Fig. 10).
415 All the above results indicate that the atmospheric aging process could significantly improve the light
416 absorption capacity of POA particles along with the evolution of haze episodes due to the "lensing
417 effect" of SIA coating.

418 **4 Conclusions and implications**

419 This study demonstrates that primary pollutants especially large amounts of POA particles
420 emitted from the residential coal and biomass burning in rural areas initiated the wintertime regional
421 haze episode in the NCP. The presence of abundant burning-related POA particles in the atmosphere
422 could further provide surfaces for heterogeneous reactions promoting the large production of SIA
423 under stagnant metrological conditions with high RH, which further elevated the pollution level.
424 Compared with the tarballs which have been confirmed as BrC with strong light-absorbing capacities
425 in previous studies (Adachi et al., 2019; C. Li et al., 2019), the spherical POA (i.e., tarball) and
426 irregular POA particles observed in this study can better represent burning-related light-absorbing
427 primary organic particles in the wintertime hazes. Therefore, the ubiquitous light-absorbing POA
428 particles in the atmosphere of NCP unquestionably affect the energy balance (Feng et al., 2013). We
429 found that burning-related POA particles remained quite stable during the regional transport from the
430 rural areas to urban Beijing in the NCP and were coated with SIA through the atmospheric aging
431 process in the haze layer, which could significantly enhance the light absorption capacity of POA
432 particles via the "lensing effect" of SIA coating. We estimated that E_{abs} values were within the upper
433 limit of 1.75 in core–shell Mie calculations considering the typical size distribution of POA particles

(200–800 nm) in the NCP. Furthermore, Alexander et al. (2008) found plenty of primary brown carbon spheres with strong light absorption capacity in East Asian outflow, which indicates that the POA particles could be transported over long distances and still retain their strong light-absorbing properties, and thus can affect the regional and even global radiative forcing. Therefore, we highlight that the "lensing effect", which has been adequately reported on BC particles but not on light-absorbing POA particles in previous studies, should be further considered on these POA particles in radiative forcing models.

Considering the adverse effects of residential coal and biomass burning on the haze formation and climate change, we suggest that the governments should continue to implement the "Clean Air Actions" (Zhang and Geng, 2019), especially encourage the use of clean energy such as electricity and natural gas for heating and cooking in rural areas of North China in winter.

Data availability

All data presented in this paper are available upon request. Please contact the corresponding author (liweijun@zju.edu.cn).

Author Contributions

WL and LL designed the research. LL performed the data analysis and wrote the manuscript and WL revised it. JZ and YZ assisted with the sample collection. YS provided the AMS data at the Beijing site. LL, JZ, YZ, LX, QY, and YW carried out the chemical analysis of $PM_{2.5}$ and TEM analysis of individual particles. ZS, YS, DL, and PF contributed to the improvement of this manuscript. All the authors approved the final version of this paper.

Competing interests

The authors declare that they have no conflict of interest.

Acknowledgements

This work was funded by the National Natural Science Foundation of China (42075096 and

91844301), National Key R&D Program of China (2017YFC0212700), Zhejiang Provincial Natural Science Foundation of China (LZ19D050001), and China Postdoctoral Science Foundation (2020M681823). Z. Shi acknowledges the UK Natural Environment Research Council (NE/S00579X/1 and NE/N007190/1). We acknowledge the NOAA Air Resources Laboratory for the provision of the HYSPLIT transport and dispersion model and READY website (http://www.ready.noaa.gov) used in this paper.

References

Adachi, K., Sedlacek, A. J., Kleinman, L., Chand, D., Hubbe, J. M., and Buseck, P. R.: Volume changes upon heating of aerosol particles from biomass burning using transmission electron microscopy, Aerosol Sci. Tech., 52, 46-56, 10.1080/02786826.2017.1373181, 2018.

Adachi, K., Sedlacek, A. J., Kleinman, L., Springston, S. R., Wang, J., Chand, D., Hubbe, J. M., Shilling, J. E., Onasch, T. B., Kinase, T., Sakata, K., Takahashi, Y., and Buseck, P. R.: Spherical tarball particles form through rapid chemical and physical changes of organic matter in biomass-burning smoke, Proc. Natl. Acad. Sci. U.S.A., 116, 19336-19341, 10.1073/pnas.1900129116, 2019.

Aden, A. L., and Kerker, M.: Scattering of Electromagnetic Waves from Two Concentric Spheres, J. Appl. Phys., 22, 1242-1246, 10.1063/1.1699834, 1951.

Alexander, D. T. L., Crozier, P. A., and Anderson, J. R.: Brown carbon spheres in East Asian outflow and their optical properties, Science, 321, 833-836, 2008.

Bohren, C. F., and Huffman, D. R.: Absorption and scattering of light by small particles, John Wiley & Sons, New York, 1983.

Bond, T. C., Habib, G., and Bergstrom, R. W.: Limitations in the enhancement of visible light absorption due to mixing state, J. Geophys. Res.-Atmos., 111, D20211, 10.1029/2006jd007315, 2006.

Bond, T. C., Doherty, S. J., Fahey, D., Forster, P., Berntsen, T., DeAngelo, B., Flanner, M., Ghan, S., Kärcher, B., and Koch, D.: Bounding the role of black carbon in the climate system: A scientific assessment, J. Geophys. Res.-Atmos., 118, 5380-5552, 10.1002/jgrd.50171, 2013.

Chakrabarty, R. K., and Heinson, W. R.: Scaling Laws for Light Absorption Enhancement Due to Nonrefractory Coating of Atmospheric Black Carbon Aerosol, Phys. Rev. Lett., 121, 218701, 10.1103/PhysRevLett.121.218701, 2018.

Chang, X., Wang, S., Zhao, B., Cai, S., and Hao, J.: Assessment of inter-city transport of particulate

matter in the Beijing–Tianjin–Hebei region, Atmos. Chem. Phys., 18, 4843-4858, 10.5194/acp-18-4843-2018, 2018.

Chen, S., Xu, L., Zhang, Y., Chen, B., Wang, X., Zhang, X., Zheng, M., Chen, J., Wang, W., Sun, Y., Fu, P., Wang, Z., and Li, W.: Direct observations of organic aerosols in common wintertime hazes in North China: insights into direct emissions from Chinese residential stoves, Atmos. Chem. Phys., 17, 1259-1270, 10.5194/acp-17-1259-2017, 2017.

Chen, X., Wang, H., Lu, K., Li, C., Zhai, T., Tan, Z., Ma, X., Yang, X., Liu, Y., Chen, S., Dong, H., Li, X., Wu, Z., Hu, M., Zeng, L., and Zhang, Y.: Field Determination of Nitrate Formation Pathway in Winter Beijing, Environ. Sci. Technol., 54, 9243-9253, 10.1021/acs.est.0c00972, 2020.

Cheng, Y., Zheng, G., Wei, C., Mu, Q., Zheng, B., Wang, Z., Gao, M., Zhang, Q., He, K., Carmichael, G., Pöschl, U., and Su, H.: Reactive nitrogen chemistry in aerosol water as a source of sulfate during haze events in China, Sci. Adv., 2, e1601530, 10.1126/sciadv.1601530, 2016.

Chylek, P., Lee, J. E., Romonosky, D. E., Gallo, F., Lou, S., Shrivastava, M., Carrico, C. M., Aiken, A. C., and Dubey, M. K.: Mie Scattering Captures Observed Optical Properties of Ambient Biomass Burning Plumes Assuming Uniform Black, Brown, and Organic Carbon Mixtures, J. Geophys. Res.-Atmos., 124, 11406-11427, 10.1029/2019jd031224, 2019.

Denjean, C., Formenti, P., Picquet-Varrault, B., Katrib, Y., Pangui, E., Zapf, P., and Doussin, J. F.: A new experimental approach to study the hygroscopic and optical properties of aerosols: application to ammonium sulfate particles, Atmos. Meas. Tech., 7, 183-197, 10.5194/amt-7-183-2014, 2014.

Du, H., Li, J., Chen, X., Wang, Z., Sun, Y., Fu, P., Li, J., Gao, J., and Wei, Y.: Modeling of aerosol property evolution during winter haze episodes over a megacity cluster in northern China: roles of regional transport and heterogeneous reactions of SO_2, Atmos. Chem. Phys., 19, 9351-9370, 10.5194/acp-19-9351-2019, 2019.

Ebert, M., Weigel, R., Kandler, K., Günther, G., Molleker, S., Grooß, J. U., Vogel, B., Weinbruch, S., and Borrmann, S.: Chemical analysis of refractory stratospheric aerosol particles collected within the arctic vortex and inside polar stratospheric clouds, Atmos. Chem. Phys., 16, 8405-8421, 10.5194/acp-16-8405-2016, 2016.

Fan, X., Liu, J., Zhang, F., Chen, L., Collins, D., Xu, W., Jin, X., Ren, J., Wang, Y., Wu, H., Li, S., Sun, Y., and Li, Z.: Contrasting size-resolved hygroscopicity of fine particles derived by HTDMA and HR-ToF-AMS measurements between summer and winter in Beijing: the impacts of aerosol aging and local emissions, Atmos. Chem. Phys., 20, 915-929, 10.5194/acp-20-915-2020, 2020.

Feng, Y., Ramanathan, V., and Kotamarthi, V. R.: Brown carbon: a significant atmospheric absorber of solar radiation?, Atmos. Chem. Phys., 13, 8607-8621, 10.5194/acp-13-8607-2013, 2013.

Hoffer, A., Toth, A., Nyiro-Kosa, I., Posfai, M., and Gelencser, A.: Light absorption properties of laboratory-generated tar ball particles, Atmos. Chem. Phys., 16, 239-246, 10.5194/acp-16-239-2016, 2016.

IPCC: Climate change 2013: The Physical Science Basis. Contribution of Working Group I to the Fifth Assessment Report of the Intergovernmental Panel on Climate Change, Cambridge University Press, Cambridge/New York, 2013.

Li, C., He, Q., Schade, J., Passig, J., Zimmermann, R., Meidan, D., Laskin, A., and Rudich, Y.: Dynamic changes in optical and chemical properties of tar ball aerosols by atmospheric photochemical aging, Atmos. Chem. Phys., 19, 139-163, 10.5194/acp-19-139-2019, 2019.

Li, H., Zhang, Q., Zhang, Q., Chen, C., Wang, L., Wei, Z., Zhou, S., Parworth, C., Zheng, B., Canonaco, F., Prevot, A. S. H., Chen, P., Zhang, H., Wallington, T. J., and He, K.: Wintertime aerosol chemistry and haze evolution in an extremely polluted city of the North China Plain: significant contribution from coal and biomass combustion, Atmos. Chem. Phys., 17, 4751-4768, 10.5194/acp-17-4751-2017, 2017.

Li, J., Han, Z., Li, J., Liu, R., Wu, Y., Liang, L., and Zhang, R.: The formation and evolution of secondary organic aerosol during haze events in Beijing in wintertime, Sci. Total Environ., 703, 134937, 10.1016/j.scitotenv.2019.134937, 2020.

Li, M., Fan, X., Zhu, M., Zou, C., Song, J., Wei, S., Jia, W., and Peng, P. a.: Abundance and Light Absorption Properties of Brown Carbon Emitted from Residential Coal Combustion in China, Environ. Sci. Technol., 53, 595-603, 10.1021/acs.est.8b05630, 2019.

Li, W., Zhou, S., Wang, X., Xu, Z., Yuan, C., Yu, Y., Zhang, Q., and Wang, W.: Integrated evaluation of aerosols from regional brown hazes over northern China in winter: Concentrations, sources, transformation, and mixing states, J. Geophys. Res.-Atmos., 116, D09301, 10.1029/2010JD015099, 2011.

Li, W., Shao, L., Zhang, D., Ro, C.-U., Hu, M., Bi, X., Geng, H., Matsuki, A., Niu, H., and Chen, J.: A review of single aerosol particle studies in the atmosphere of East Asia: morphology, mixing state, source, and heterogeneous reactions, J. Clean Prod., 112, 1330-1349, 10.1016/j.jclepro.2015.04.050, 2016a.

Li, W., Sun, J., Xu, L., Shi, Z., Riemer, N., Sun, Y., Fu, P., Zhang, J., Lin, Y., and Wang, X.: A conceptual framework for mixing structures in individual aerosol particles, J. Geophys. Res.-Atmos., 121, 13784-13798, 10.1002/2016JD025252, 2016b.

Li, X., Yang, Y., Liu, S., Zhao, Q., Wang, G., and Wang, Y.: Light absorption properties of brown carbon (BrC) in autumn and winter in Beijing: Composition, formation and contribution of nitrated aromatic compounds, Atmos. Environ., 223, 117289, 10.1016/j.atmosenv.2020.117289,

2020.

Lin, P., Aiona, P. K., Li, Y., Shiraiwa, M., Laskin, J., Nizkorodov, S. A., and Laskin, A.: Molecular Characterization of Brown Carbon in Biomass Burning Aerosol Particles, Environ. Sci. Technol., 50, 11815-11824, 10.1021/acs.est.6b03024, 2016.

Liu, D., Whitehead, J., Alfarra, M. R., Reyes-Villegas, E., Spracklen, D. V., Reddington, C. L., Kong, S., Williams, P. I., Ting, Y.-C., Haslett, S., Taylor, J. W., Flynn, M. J., Morgan, W. T., McFiggans, G., Coe, H., and Allan, J. D.: Black-carbon absorption enhancement in the atmosphere determined by particle mixing state, Nat. Geosci., 10, 184-188, 10.1038/ngeo2901, 2017.

Liu, J., Mauzerall, D. L., Chen, Q., Zhang, Q., Song, Y., Peng, W., Klimont, Z., Qiu, X., Zhang, S., Hu, M., Lin, W., Smith, K. R., and Zhu, T.: Air pollutant emissions from Chinese households: A major and underappreciated ambient pollution source, Proc. Natl. Acad. Sci. U.S.A., 113, 7756-7761, 10.1073/pnas.1604537113, 2016.

Liu, L., Kong, S., Zhang, Y., Wang, Y., Xu, L., Yan, Q., Lingaswamy, A. P., Shi, Z., Lv, S., Niu, H., Shao, L., Hu, M., Zhang, D., Chen, J., Zhang, X., and Li, W.: Morphology, composition, and mixing state of primary particles from combustion sources — crop residue, wood, and solid waste, Sci. Rep., 7, 5047, 10.1038/s41598-017-05357-2, 2017.

Liu, L., Zhang, J., Xu, L., Yuan, Q., Huang, D., Chen, J., Shi, Z., Sun, Y., Fu, P., Wang, Z. F., Zhang, D., and Li, W.: Cloud scavenging of anthropogenic refractory particles at a mountain site in North China, Atmos. Chem. Phys., 18, 14681-14693, 10.5194/acp-18-14681-2018, 2018.

Liu, P., Zhang, C., Xue, C., Mu, Y., Liu, J., Zhang, Y., Tian, D., Ye, C., Zhang, H., and Guan, J.: The contribution of residential coal combustion to atmospheric $PM_{2.5}$ in northern China during winter, Atmos. Chem. Phys., 17, 11503-11520, 10.5194/acp-17-11503-2017, 2017.

Liu, P., Ye, C., Xue, C., Zhang, C., Mu, Y., and Sun, X.: Formation mechanisms of atmospheric nitrate and sulfate during the winter haze pollution periods in Beijing: gas-phase, heterogeneous and aqueous-phase chemistry, Atmos. Chem. Phys., 20, 4153-4165, 10.5194/acp-20-4153-2020, 2020.

Ma, Q., Wu, Y., Zhang, D., Wang, X., Xia, Y., Liu, X., Tian, P., Han, Z., Xia, X., Wang, Y., and Zhang, R.: Roles of regional transport and heterogeneous reactions in the $PM_{2.5}$ increase during winter haze episodes in Beijing, Sci. Total Environ., 599, 246-253, 10.1016/j.scitotenv.2017.04.193, 2017.

Pósfai, M., Simonics, R., Li, J., Hobbs, P. V., and Buseck, P. R.: Individual aerosol particles from biomass burning in southern Africa: 1. Compositions and size distributions of carbonaceous particles, J. Geophys. Res.-Atmos., 108, 8483, 10.1029/2002JD002291, 2003.

Reid, J. P., Bertram, A. K., Topping, D. O., Laskin, A., Martin, S. T., Petters, M. D., Pope, F. D., and Rovelli, G.: The viscosity of atmospherically relevant organic particles, Nat. Commun., 9, 956,

10.1038/s41467-018-03027-z, 2018.

Riemer, N., Ault, A. P., West, M., Craig, R. L., and Curtis, J. H.: Aerosol Mixing State: Measurements, Modeling, and Impacts, Rev. Geophys., 57, 187-249, 10.1029/2018rg000615, 2019.

Seinfeld, J. H., and Pandis, S. N.: Atmospheric chemistry and physics: from air pollution to climate change, John Wiley & Sons, 2006.

Shi, Z., Vu, T., Kotthaus, S., Harrison, R. M., Grimmond, S., Yue, S., Zhu, T., Lee, J., Han, Y., Demuzere, M., Dunmore, R. E., Ren, L., Liu, D., Wang, Y., Wild, O., Allan, J., Acton, W. J., Barlow, J., Barratt, B., Beddows, D., Bloss, W. J., Calzolai, G., Carruthers, D., Carslaw, D. C., Chan, Q., Chatzidiakou, L., Chen, Y., Crilley, L., Coe, H., Dai, T., Doherty, R., Duan, F., Fu, P., Ge, B., Ge, M., Guan, D., Hamilton, J. F., He, K., Heal, M., Heard, D., Hewitt, C. N., Hollaway, M., Hu, M., Ji, D., Jiang, X., Jones, R., Kalberer, M., Kelly, F. J., Kramer, L., Langford, B., Lin, C., Lewis, A. C., Li, J., Li, W., Liu, H., Liu, J., Loh, M., Lu, K., Lucarelli, F., Mann, G., McFiggans, G., Miller, M. R., Mills, G., Monk, P., Nemitz, E., O'Connor, F., Ouyang, B., Palmer, P. I., Percival, C., Popoola, O., Reeves, C., Rickard, A. R., Shao, L., Shi, G., Spracklen, D., Stevenson, D., Sun, Y., Sun, Z., Tao, S., Tong, S., Wang, Q., Wang, W., Wang, X., Wang, X., Wang, Z., Wei, L., Whalley, L., Wu, X., Wu, Z., Xie, P., Yang, F., Zhang, Q., Zhang, Y., Zhang, Y., and Zheng, M.: Introduction to the special issue “In-depth study of air pollution sources and processes within Beijing and its surrounding region (APHH-Beijing)”, Atmos. Chem. Phys., 19, 7519-7546, 10.5194/acp-19-7519-2019, 2019.

Song, J., Li, M., Jiang, B., Wei, S., Fan, X., and Peng, P. a.: Molecular Characterization of Water-Soluble Humic like Substances in Smoke Particles Emitted from Combustion of Biomass Materials and Coal Using Ultrahigh-Resolution Electrospray Ionization Fourier Transform Ion Cyclotron Resonance Mass Spectrometry, Environ. Sci. Technol., 52, 2575-2585, 10.1021/acs.est.7b06126, 2018.

Stein, A. F., Draxler, R. R., Rolph, G. D., Stunder, B. J. B., Cohen, M. D., and Ngan, F.: NOAA’s HYSPLIT Atmospheric Transport and Dispersion Modeling System, Bull. Amer. Meteorol. Soc., 96, 2059-2077, 10.1175/bams-d-14-00110.1, 2016.

Sun, J., Zhi, G., Hitzenberger, R., Chen, Y., Tian, C., Zhang, Y., Feng, Y., Cheng, M., Zhang, Y., Cai, J., Chen, F., Qiu, Y., Jiang, Z., Li, J., Zhang, G., and Mo, Y.: Emission factors and light absorption properties of brown carbon from household coal combustion in China, Atmos. Chem. Phys., 17, 4769-4780, 10.5194/acp-17-4769-2017, 2017.

Sun, Y., Jiang, Q., Wang, Z., Fu, P., Li, J., Yang, T., and Yin, Y.: Investigation of the sources and evolution processes of severe haze pollution in Beijing in January 2013, J. Geophys. Res.-Atmos., 119, 4380-4398, 10.1002/2014jd021641, 2014.

625 Sun, Y., Chen, C., Zhang, Y., Xu, W., Zhou, L., Cheng, X., Zheng, H., Ji, D., Li, J., Tang, X., Fu, P.,
626 and Wang, Z.: Rapid formation and evolution of an extreme haze episode in Northern China
627 during winter 2015, Sci. Rep., 6, 27151, 10.1038/srep27151, 2016.
628 Toon, O. B., and Ackerman, T. P.: Algorithms for the calculation of scattering by stratified spheres,
629 Appl. Opt., 20, 3657-3660, 10.1364/ao.20.003657, 1981.
630 Wang, B., Harder, T. H., Kelly, S. T., Piens, D. S., China, S., Kovarik, L., Keiluweit, M., Arey, B. W.,
631 Gilles, M. K., and Laskin, A.: Airborne soil organic particles generated by precipitation, Nat.
632 Geosci., 9, 433-437, 10.1038/NGEO2705, 2016.
633 Wang, J., Nie, W., Cheng, Y., Shen, Y., Chi, X., Wang, J., Huang, X., Xie, Y., Sun, P., Xu, Z., Qi, X.,
634 Su, H., and Ding, A.: Light absorption of brown carbon in eastern China based on 3-year multi-
635 wavelength aerosol optical property observations and an improved absorption Ångström exponent
636 segregation method, Atmos. Chem. Phys., 18, 9061-9074, 10.5194/acp-18-9061-2018, 2018.
637 Wang, J., Li, J., Ye, J., Zhao, J., Wu, Y., Hu, J., Liu, D., Nie, D., Shen, F., Huang, X., Huang, D. D.,
638 Ji, D., Sun, X., Xu, W., Guo, J., Song, S., Qin, Y., Liu, P., Turner, J. R., Lee, H. C., Hwang, S.,
639 Liao, H., Martin, S. T., Zhang, Q., Chen, M., Sun, Y., Ge, X., and Jacob, D. J.: Fast sulfate
640 formation from oxidation of SO_2 by NO_2 and HONO observed in Beijing haze, Nat. Commun.,
641 11, 2844, 10.1038/s41467-020-16683-x, 2020.
642 Wang, X., Heald, C. L., Ridley, D. A., Schwarz, J. P., Spackman, J. R., Perring, A. E., Coe, H., Liu,
643 D., and Clarke, A. D.: Exploiting simultaneous observational constraints on mass and absorption
644 to estimate the global direct radiative forcing of black carbon and brown carbon, Atmos. Chem.
645 Phys., 14, 10989-11010, 10.5194/acp-14-10989-2014, 2014.
646 Wang, Y., Liu, F., He, C., Bi, L., Cheng, T., Wang, Z., Zhang, H., Zhang, X., Shi, Z., and Li, W.:
647 Fractal Dimensions and Mixing Structures of Soot Particles during Atmospheric Processing,
648 Environ. Sci. Technol. Lett., 4, 487-493, 10.1021/acs.estlett.7b00418, 2017.
649 West, J. J., Cohen, A., Dentener, F., Brunekreef, B., Zhu, T., Armstrong, B., Bell, M. L., Brauer, M.,
650 Carmichael, G., and Costa, D. L.: What We Breathe Impacts Our Health: Improving
651 Understanding of the Link between Air Pollution and Health, Environ. Sci. Technol., 50, 4895-
652 4904, 10.1021/acs.est.5b03827, 2016.
653 Wu, C., Wu, D., and Yu, J. Z.: Quantifying black carbon light absorption enhancement with a novel
654 statistical approach, Atmos. Chem. Phys., 18, 289-309, 10.5194/acp-18-289-2018, 2018.
655 Xie, C., Xu, W., Wang, J., Wang, Q., Liu, D., Tang, G., Chen, P., Du, W., Zhao, J., Zhang, Y., Zhou,
656 W., Han, T., Bian, Q., Li, J., Fu, P., Wang, Z., Ge, X., Allan, J., Coe, H., and Sun, Y.: Vertical
657 characterization of aerosol optical properties and brown carbon in winter in urban Beijing, China,
658 Atmos. Chem. Phys., 19, 165-179, 10.5194/acp-19-165-2019, 2019.

659 Xing, L., Fu, T. M., Cao, J. J., Lee, S. C., Wang, G. H., Ho, K. F., Cheng, M. C., You, C. F., and Wang,
660 T. J.: Seasonal and spatial variability of the OM/OC mass ratios and high regional correlation
661 between oxalic acid and zinc in Chinese urban organic aerosols, Atmos. Chem. Phys., 13, 4307-
662 4318, 10.5194/acp-13-4307-2013, 2013.
663 Xu, J., Srivastava, D., Wu, X., Hou, S., Vu, T. V., Liu, D., Sun, Y., Vlachou, A., Moschos, V., Salazar,
664 G., Szidat, S., Prevot, A., Fu, P., Harrison, R. M., and Shi, Z.: An evaluation of source
665 apportionment of fine OC and $PM_{2.5}$ by multiple methods: APHH-Beijing campaigns as a case
666 study, Faraday Discussions, 10.1039/D0FD00095G, 2020.
667 Xu, W., Sun, Y., Wang, Q., Zhao, J., Wang, J., Ge, X., Xie, C., Zhou, W., Du, W., Li, J., Fu, P., Wang,
668 Z., Worsnop, D. R., and Coe, H.: Changes in Aerosol Chemistry From 2014 to 2016 in Winter in
669 Beijing: Insights From High-Resolution Aerosol Mass Spectrometry, J. Geophys. Res.-Atmos.,
670 124, 1132-1147, 10.1029/2018jd029245, 2019.
671 Yan, C., Zheng, M., Bosch, C., Andersson, A., Desyaterik, Y., Sullivan, A. P., Collett, J. L., Zhao, B.,
672 Wang, S., He, K., and Gustafsson, Ö.: Important fossil source contribution to brown carbon in
673 Beijing during winter, Sci. Rep., 7, 43182, 10.1038/srep43182, 2017.
674 Yu, H., Li, W., Zhang, Y., Tunved, P., Dall'Osto, M., Shen, X., Sun, J., Zhang, X., Zhang, J., and Shi,
675 Z.: Organic coating on sulfate and soot particles during late summer in the Svalbard Archipelago,
676 Atmos. Chem. Phys., 19, 10433-10446, 10.5194/acp-19-10433-2019, 2019.
677 Zhang, J., Liu, L., Wang, Y., Ren, Y., Wang, X., Shi, Z., Zhang, D., Che, H., Zhao, H., Liu, Y., Niu,
678 H., Chen, J., Zhang, X., Lingaswamy, A. P., Wang, Z., and Li, W.: Chemical composition, source,
679 and process of urban aerosols during winter haze formation in Northeast China, Environ. Pollut.,
680 231, 357-366, 10.1016/j.envpol.2017.07.102, 2017.
681 Zhang, J., Liu, L., Xu, L., Lin, Q., Zhao, H., Wang, Z., Guo, S., Hu, M., Liu, D., Shi, Z., Huang, D.,
682 and Li, W.: Exploring wintertime regional haze in northeast China: role of coal and biomass
683 burning, Atmos. Chem. Phys., 20, 5355-5372, 10.5194/acp-20-5355-2020, 2020.
684 Zhang, Q., and Geng, G.: Impact of clean air action on $PM_{2.5}$ pollution in China, Sci. China-Earth
685 Sci., 62, 1845-1846, 10.1007/s11430-019-9531-4, 2019.
686 Zhang, Y., Yuan, Q., Huang, D., Kong, S., Zhang, J., Wang, X., Lu, C., Shi, Z., Zhang, X., Sun, Y.,
687 Wang, Z., Shao, L., Zhu, J., and Li, W.: Direct observations of fine primary particles from
688 residential coal burning: insights into their morphology, composition, and hygroscopicity, J.
689 Geophys. Res.-Atmos., 123, 12964-12979, 10.1029/2018JD028988, 2018.
690 Zheng, G. J., Duan, F. K., Su, H., Ma, Y. L., Cheng, Y., Zheng, B., Zhang, Q., Huang, T., Kimoto, T.,
691 Chang, D., Pöschl, U., Cheng, Y. F., and He, K. B.: Exploring the severe winter haze in Beijing:
692 the impact of synoptic weather, regional transport and heterogeneous reactions, Atmos. Chem.

693 Phys., 15, 2969-2983, 10.5194/acp-15-2969-2015, 2015.
694 Zhong, J., Zhang, X., Wang, Y., Wang, J., Shen, X., Zhang, H., Wang, T., Xie, Z., Liu, C., Zhang, H.,
695 Zhao, T., Sun, J., Fan, S., Gao, Z., Li, Y., and Wang, L.: The two-way feedback mechanism
696 between unfavorable meteorological conditions and cumulative aerosol pollution in various haze
697 regions of China, Atmos. Chem. Phys., 19, 3287-3306, 10.5194/acp-19-3287-2019, 2019.
698

Figures

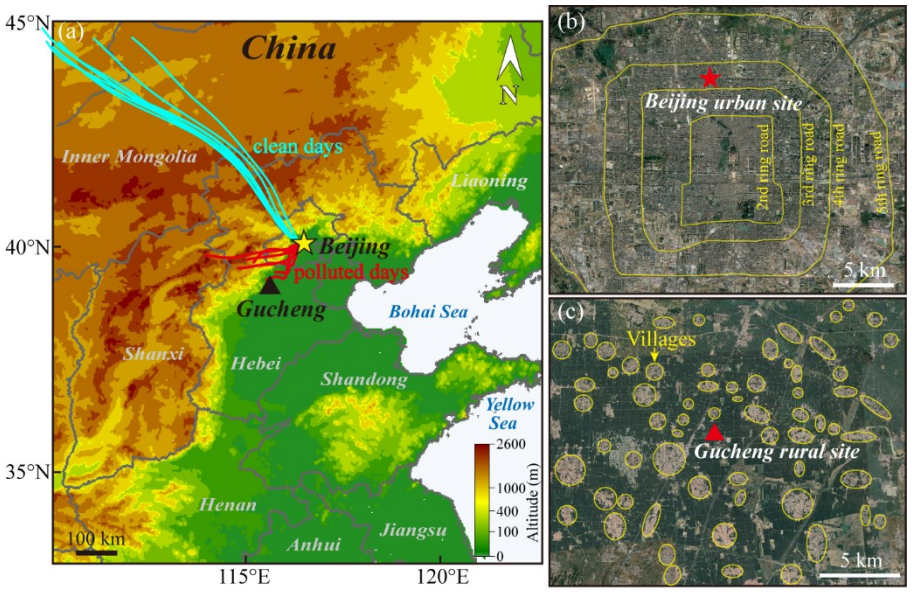

Figure 1. Locations of Beijing and Gucheng in the North China Plain (a) and the expanded view of surrounding topographies around the Beijing urban site (b) and Gucheng rural site (c). The 24-h backward trajectories of air masses ending at the height of 100 m (a.g.l) over the Beijing urban site in clean and polluted days during 20–27 November, 2020 are also shown in (a). (Map copyright @2020 Google Maps)

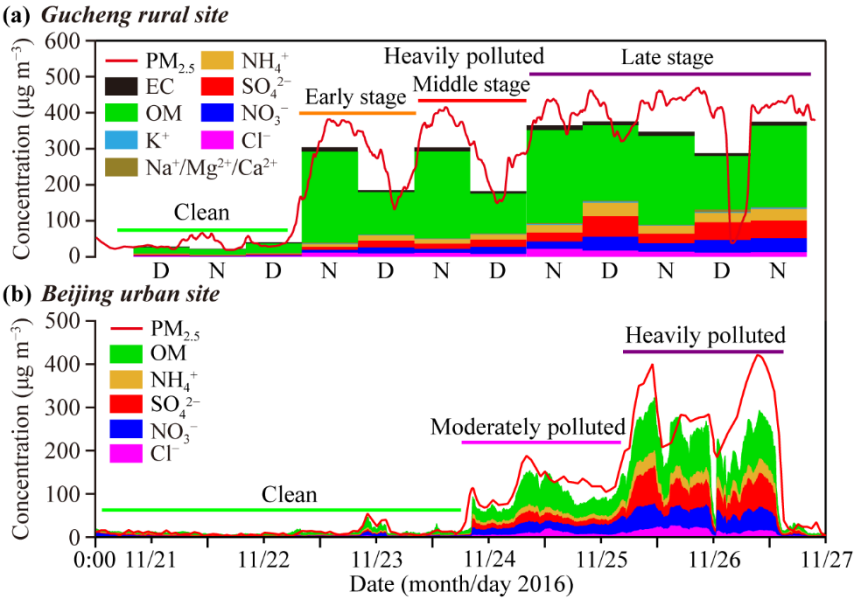

Figure 2. Time series of $PM_{2.5}$ and major aerosol chemical species at the (a) Gucheng rural site and (b) Beijing urban site. Chemical species were obtained by offline analysis of daytime (D) and nighttime (N) $PM_{2.5}$ filter samples at the rural site and were obtained by online analysis of NR-PM_1 using a high-resolution aerosol mass spectrometer (HR-AMS) at the urban site. The different periods of the haze episode at rural and urban sites are marked in this figure.

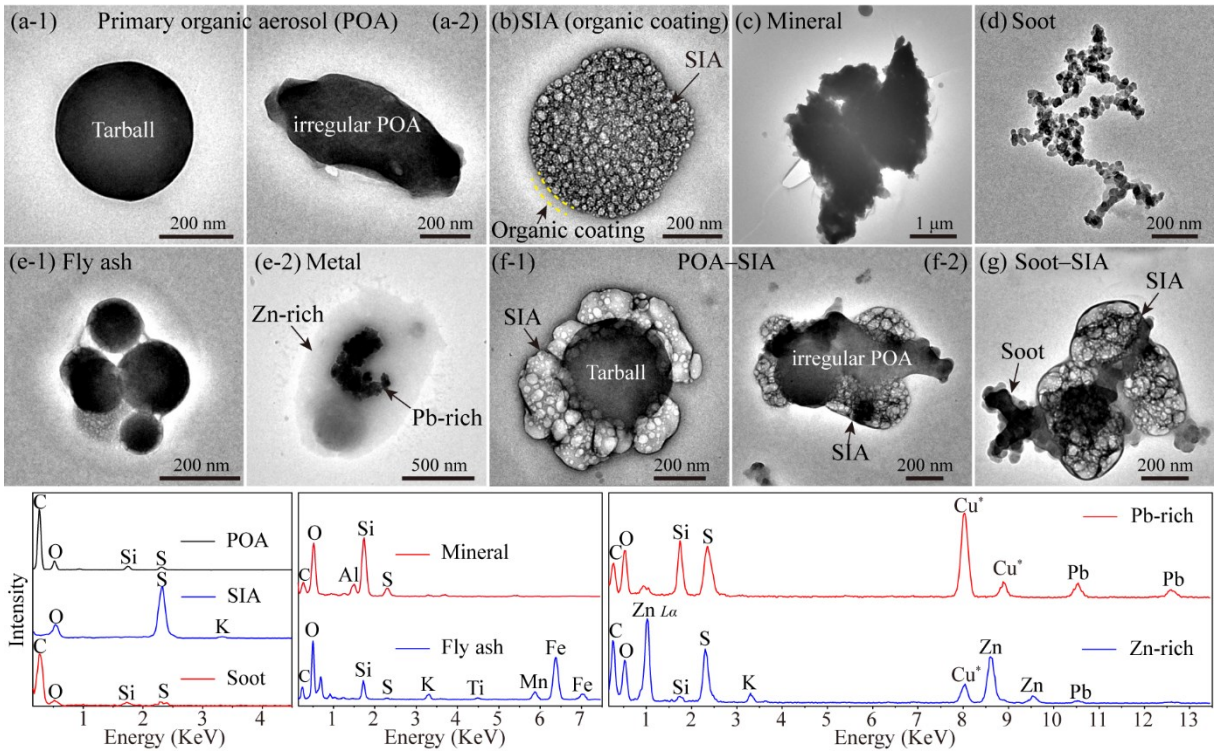

Figure 3. Typical transmission electron microscopy (TEM) images and energy-dispersive X-ray spectrometry (EDS) spectra showing the morphology, composition, and mixing structures of different individual particle types. (a) primary organic aerosol (POA) particles with (a-1) spherical (i.e., tarball) or (a-2) irregular shapes; (b) secondary inorganic aerosol (SIA) particle with secondary organic coating; (c) mineral; (d) soot; (e-1) fly ash and (e-2) metal; (f) internally mixed POA particle with SIA coating (POA–SIA); (g) internally mixed soot particle with SIA coating (soot–SIA).

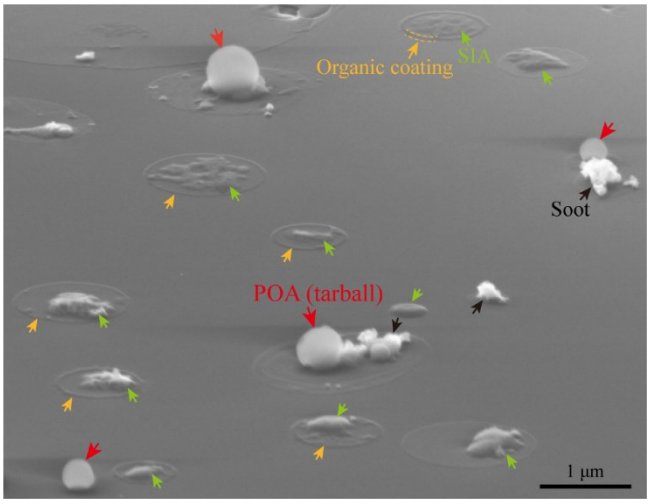

Figure 4. Scanning electron microscopy (SEM) image acquired in the secondary electron (SE2) mode at a 75° tilt angle showing the surface morphology of individual particles in the vertical dimension. The red, black, green, and orange arrows indicate primary organic aerosol (POA) particle (mainly tarball), soot particle, secondary inorganic aerosol (SIA) particle, and secondary organic coating, respectively.

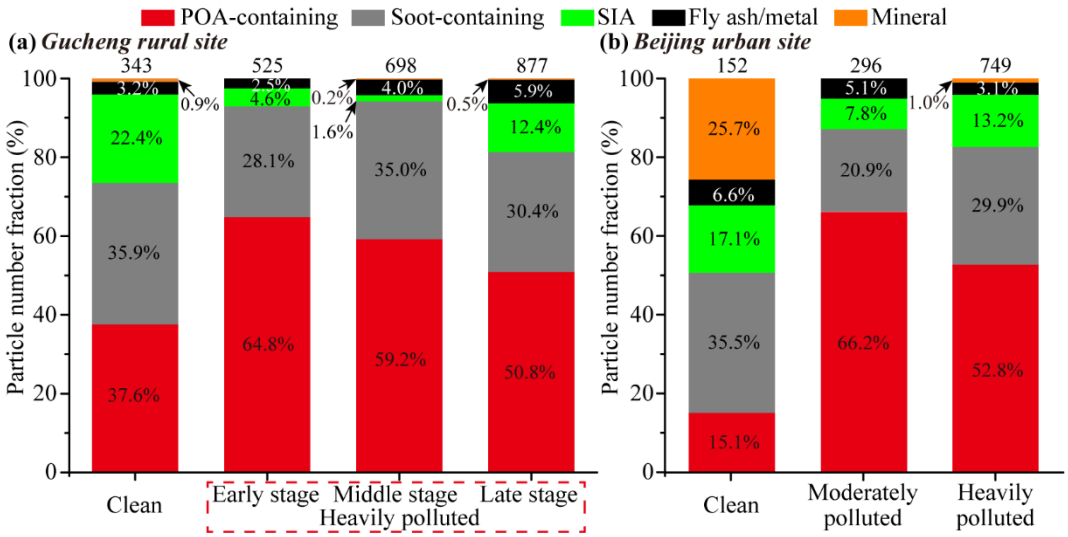

Figure 5. Relative abundance of different particle types in different periods at the (a) Gucheng rural site and (b) Beijing urban site. The numbers of analyzed particles in different periods are shown on the top of each column.

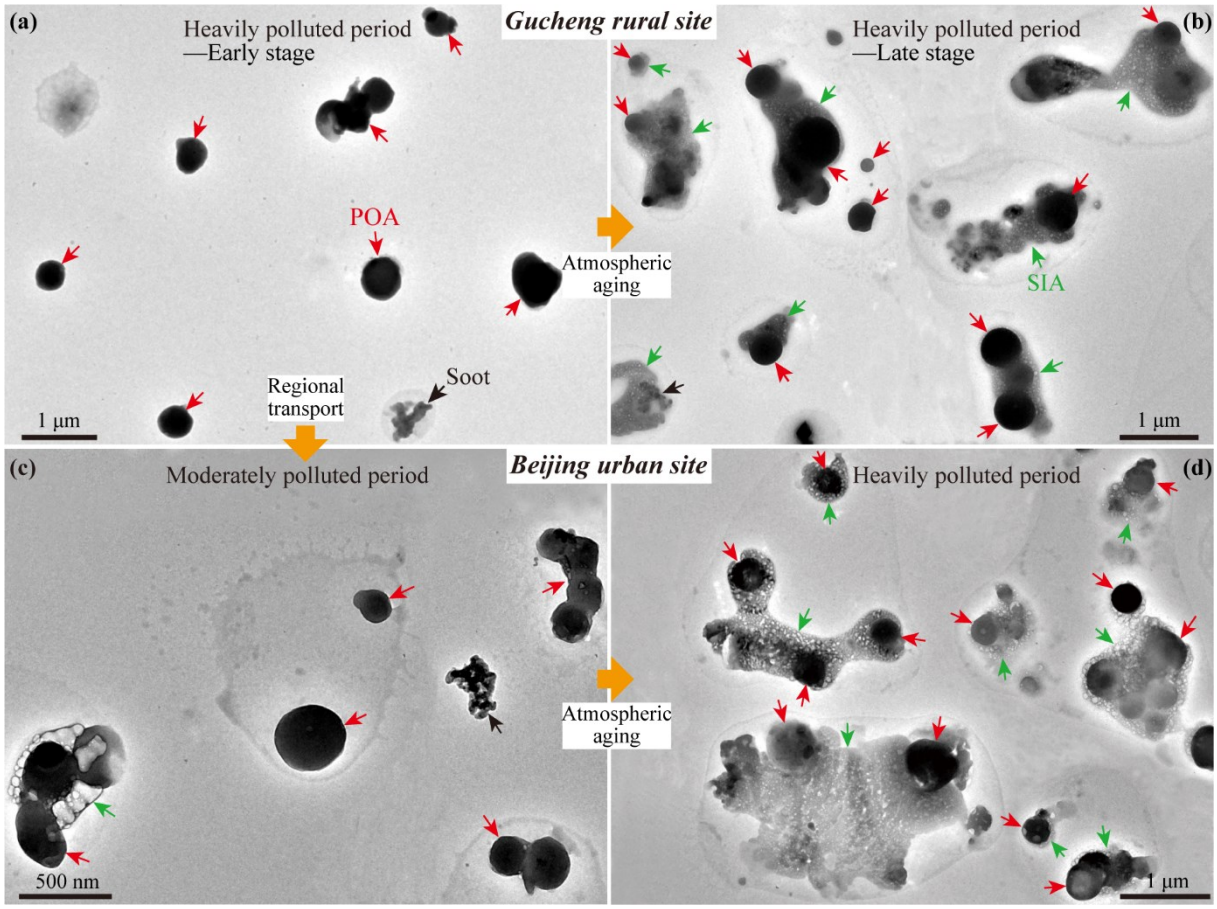

Figure 6. TEM images showing individual particles collected in the (a) early stage and (b) late stage of heavily polluted period at the Gucheng rural site and in the (c) moderately polluted and (d) heavily polluted periods at the Beijing urban site. The red, green, and black arrows indicate primary organic aerosol (POA) particle, secondary inorganic aerosol (SIA) particle, and soot particle, respectively.

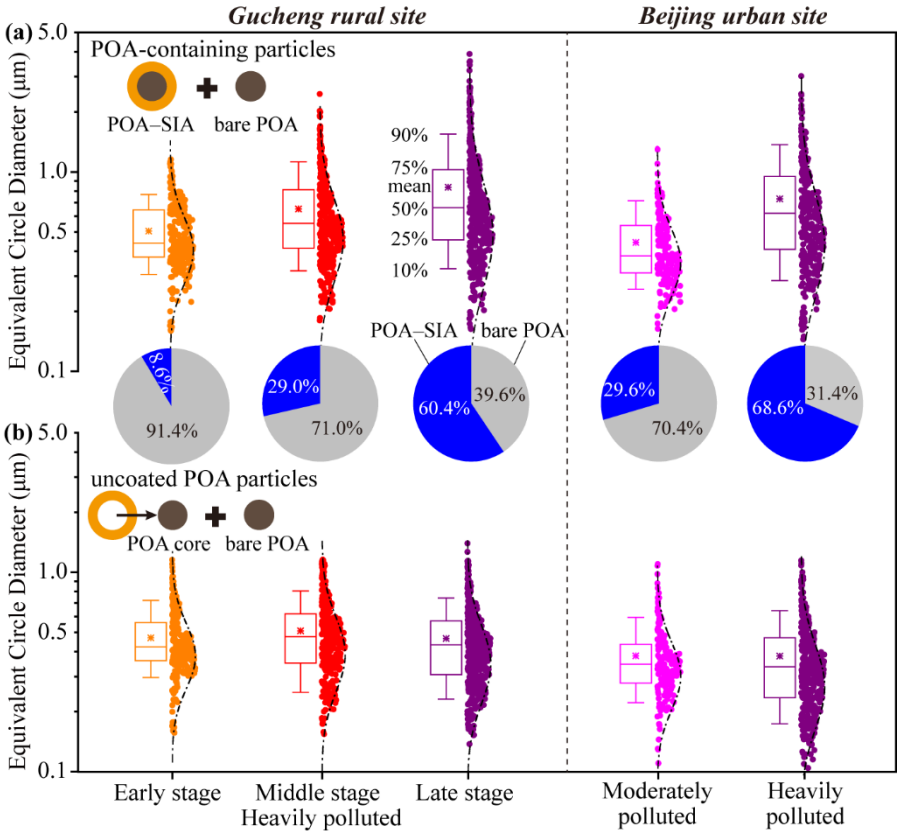

Figure 7. Box plots showing equivalent circle diameters (ECD) of (a) POA-containing particles (including core–shell POA–SIA and bare POA) and (b) uncoated POA particles (including POA cores without SIA shell and bare POA) in different polluted periods at the Gucheng rural site and Beijing urban site. The solid circles (right of the box) represent the ECD of individual particles with lognormal distributions. The pie charts present the relative number fractions between POA–SIA and bare POA in different polluted periods.

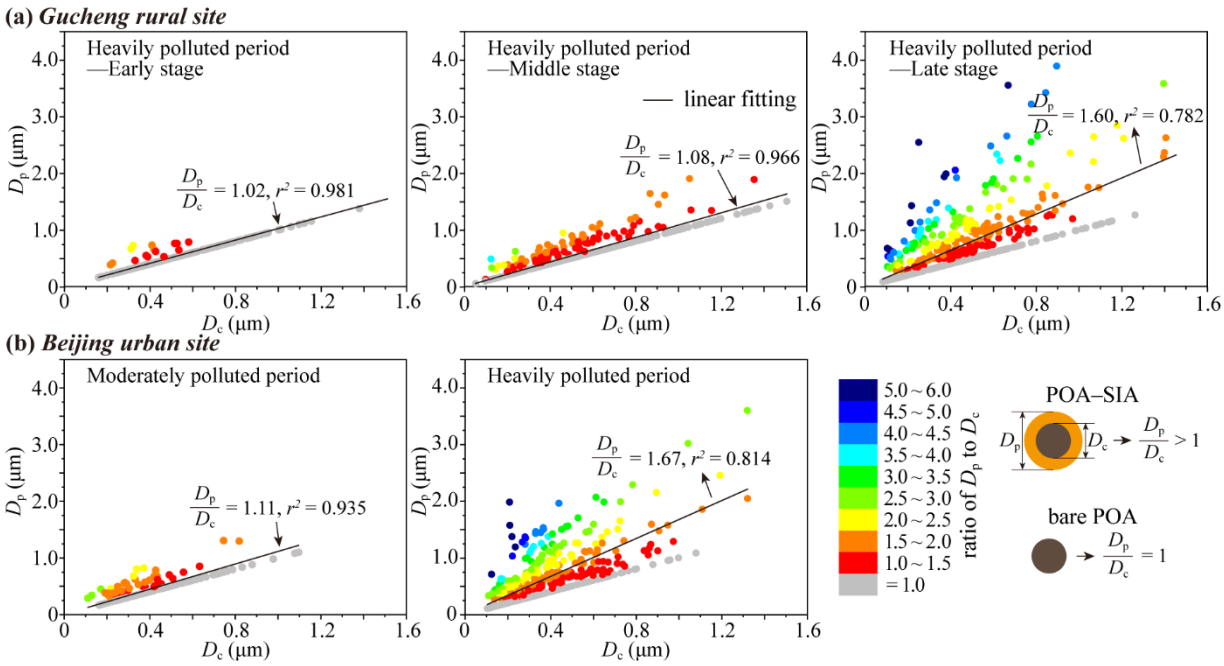

Figure 8. Relationship between the diameter of POA-containing particle (D_p) and its POA core (D_c) in the early stage, middle stage, and late stage of heavily polluted period at the Gucheng rural site (a) and in the moderately polluted and heavily polluted periods at the Beijing urban site (b).

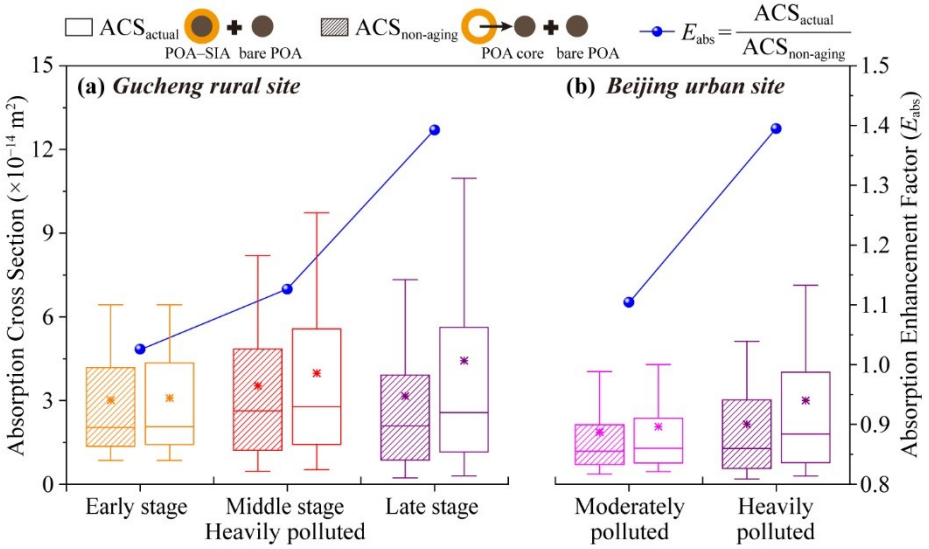

741

742 Figure 9. Box plots of light absorption cross sections (ACS) of individual POA-containing particles (including core–
743 shell POA–SIA and bare POA) under the actual scenario (ACS_{actual}) and uncoated POA particles (including POA
744 cores without SIA shell and bare POA) under the particle non-aging scenario ($ACS_{non\text{-}aging}$) at the wavelength of 550
745 nm; and variations in the light absorption enhancement factors (E_{abs}, i.e., ratio of ACS_{actual} to $ACS_{non\text{-}aging}$) in different
746 polluted periods at the (a) Gucheng rural site and (b) Beijing urban site. A refractive index of 1.55−0i for non-light-
747 absorbing SIA coating (Denjean et al., 2014) and 1.67−0.27i for light-absorbing POA core (Alexander et al., 2008)
748 were adopted at the wavelength of 550 nm. The box represents the 25th (lower line), 50th (middle line), and 75th
749 (top line) percentiles; the asterisk in the box represents the mean value; and the end lines of the vertical bars
750 represent the 10th (below the box) and 90th (above the box) percentiles.

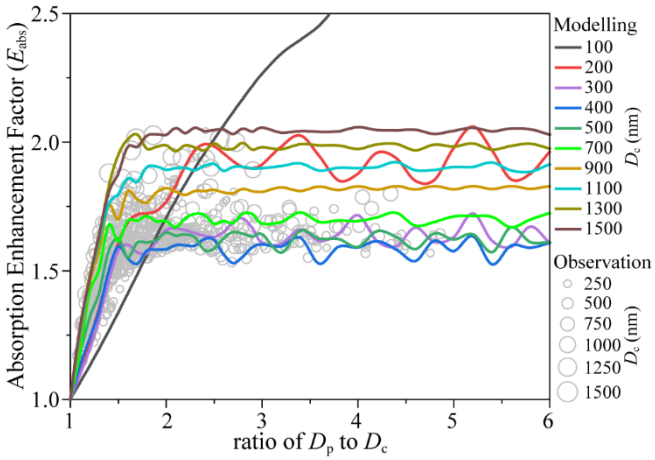

Figure 10. Mie theory-calculated light absorption enhancement factors (E_{abs}) of modeled core–shell POA–SIA particles (i.e., ratio of $ACS_{POA–SIA}$ to $ACS_{POA\ pore}$) with different POA core diameters (D_c) as a function of particle-to-core diameter ratio (D_p/D_c) at the wavelength of 550 nm (solid lines). A refractive index of 1.55−0i for non-light-absorbing SIA coating (Denjean et al., 2014) and 1.67−0.27i for light-absorbing POA core (Alexander et al., 2008) were adopted at the wavelength of 550 nm. The open circles represent all the observed POA–SIA particles during the whole polluted periods at Gucheng rural and Beijing urban sites.